REPUBLIC OF AZERBAIJAN

On the rights of the manuscript

ABSTRACT

of the dissertation for the degree of Doctor of Science

THE EFFECTS OF HEAVY ION, NEUTRON AND IONIZING IRRADIATION ON THE STRUCTURAL CHANGES AND THERMOPHYSICAL PROPERTIES OF BORON BASED COMPOUNDS

Specialty: 2225.01 Radiation materials science

Field of science: Physics

Applicant: Matlab Nabi oglu Mirzayev

Baku – 2022

The work was performed at Institute of Radiation Problems of Azerbaijan National Academy of Sciences

Scientific adviser: Correspondent member of ANAS, professor
Ogtay Abil oglu Samadov

Official opponents:

Doctor of Physical and Mathematical Sciences, Professor
Ogtay Kazim oglu Gasimov

Doctor of Physical Sciences, Professor
Adil Polad oglu Abdullayev

Doctor of Physical Sciences, Professor
Rauf Madat oglu Sardarli

Doctor of Physical Sciences, Associate Professor
Rafiga Zabil gizi Mehdiyeva

Dissertation council BED 1.21 of Supreme Attestation Commission under the President of the Republic of Azerbaijan operating at Institute of Radiation Problems of Azerbaijan National Academy of Sciences

Chairman of the Dissertation council:

Correspondent member of ANAS
Doctor of Physical and
Mathematical Sciences, Professor
Rahim Abil oglu Madatov

Scientific secretary of the Dissertation council:

Doctor of Philosophy on Physics
Muslum Ahmad oglu Mammadov

Chairman of the scientific seminar:

Doctor of Physical Sciences,
Associate Professor
Matanat Ahmad gizi Mehrabova

GENERAL CHARACTERISTICS OF THE WORK

The actuality of the subject. The main priorities of irradiation materialism in solid state physics are based on the study of irradiation defects formed in the crystal structure, the transfer of kinetic energy carried by different types of particles to the crystal structure, study of the kinetics of energy distribution along the volume of the structure and the study of final processes.

The basic principles of irradiation processes are based on a chain of processes. The probability of simultaneous occurrence of processes is analyzed by the transition of the extinct process to a new mechanism through external influences. Interaction of high-energy particles with atoms in a crystalline structure, transfer of kinetic energy to atoms located in the nodes of the crystal lattice, formation of the first cascade of exposed atoms, coordinate and directional displacement of atoms in the crystalline structure, depends on the kinetics of processes occurring by a complex mechanism, such as the formation of vacancies, interatomic nodes, point defects, and disturbances between near and far atoms. It is widely used in the manufacture of neutron absorbers in nuclear reactors, in optical devices, in the manufacture of detectors for neutrons of different energies. Based on all the superior properties listed for Boron compounds and the scientific results obtained from research published in recent years, the topic of the dissertation is based on four main compounds B_4C, BN, B_6Si and B_2O_3.

The durable chemical, physical and mechanical properties of the boron carbide (B_4C) sample, which has been extensively studied in the study, have created extensive opportunities for its application in modern nuclear technologies. According to the kinetics of thermophysical properties, boron carbide is a material resistant to high temperatures (melting point 2350°C, evaporation temperature 3500°C). Boron carbide with a unique crystalline structure (high mechanical strength at a low density of 2.52 g/cm^3) is widely used in nuclear reactors as "rods that control the kinetics of fuels". B_4C is of great interest in the development of highly chemically resistant and protective coatings in the military industry in various aggressive environments. The use of BN and B_6Si samples as detectors over a

wide temperature range has been of great interest due to their neutron and gamma ray properties and high oxidation temperatures. The high thermophysical properties (heat capacity, thermal conductivity, thermodiffusion coefficient) of composite compounds formed by boron nitride compounds with SiC, ZrB, AlN ceramic compounds further expand its field of application.

The oxidation resistance of composite materials formed by boron nitride with boron carbide, which forms a porous structure, is ten times higher than that of a pure boron carbide sample, and the microstructural structure and properties of the compounds are very suitable for engineering requirements. Gamma rays have been shown to create cubic BN phase traces in the hexagonal boron nitride structure, to change the hybridization form of the crystal structure, and to form a complex thermodynamic mechanism at high temperatures. In the boron silicate samples, the activation energy of vacancies, the displacement of free boron and silicon atoms in the crystal structure, the change in Gibbs energy, enthalpy and entropy according to a complex law have led to the use of the compound over a wide temperature range.

One of the objects of research, the B_2O_3 sample with a trigonal spatial structure, has applications in nuclear technology, solar energy processing, electronic devices and acoustic-optical devices. High results are obtained in the optical properties of boron oxide compounds and in the optical properties and signal transmission efficiency of complex composite compounds formed with SiO_2 and Si as the base matrix. In the process of focusing ionizing irradiation is widely used in the preparation of boron oxide nanoparticles and optical fibers with high transmittance.

Compounds formed by B_2O_3 samples with boron silicates at different molar concentrations are widely used for optical lenses with high refractive index and low refractive index. A number of studies providing information on new functional groups of optical parameters, boron oxide compounds under conditions of irirradiation with high-intensity neutron flow, show that there is a great need to study the change in thermodynamic properties under the influence of temperature. An experimental study of temperature-dependent

transitions in boron compounds to clarify all these aspects and problems, clarifying the mechanism of thermophysical effects under the influence of various irradiation is a key component of the research.

The purpose of the dissertation- is structural transformations in samples of boron basid compounds under the influence of fast neutrons, high-energy heavy ions, electron flow and gamma rays mechanism of change of thermal function, thermodynamic functions, oxidation kinetics and the study of mathematical substantiation.

In order to achieve the goals indicated in the research, the following issues are to be addressed:

1. Obtaining high-purity research materials (US Research Nanomaterial, Inc., TX, USA and Sky Spring Nanomaterials, USA, Sigma-Aldrich);

2. Carrying out structural analyzes in research samples;

3. Irradiation of samples with fast neutrons with energy E <1 MeV at room temperature at intensities 4.0×10^{12} n/(cm²×sec), 8.0×10^{12} n/(cm²× sec), 1.37×10^{13} n/(cm²×sec), 4.0×10^{14} n/(cm²×sec) and 1.0×10^{15} n/(cm²× sec);

4. Irradiation at 4.16×10^{16} 1/cm^2, 1.20×10^{17} 1/cm^2 and 1.03×10^{18} 1/cm^2 intensities in 2.5 MeV linear electronic accelerator;

5. Irradiation with ^{132}Xe ions with an energy of 167 MeV at an intensity of 5.0×10^{12} ion/cm^2, 5.0×10^{13} ion/cm^2 and 3.83×10^{14} ion/cm^2;

6. Irradiation at absorption doses of 9.7 kGy, 48.5 kGy, 97 kGy, 145.5 kGy and 194 kGy with ^{60}Co source with 1.17 MeV and 1.33 MeV energy lines;

7. Structural analysis of irradiated samples by “structural analysis method”;

8. Study of B_4C, BN, B_6Si and B_2O_3 samples by Raman and IR spectroscopic methods;

9. Analysis of surface morphology of research samples with atomic force microscopy after irirradiation with fast heavy ions;

10. SRIM-code analysis of B_4C, BN, B_6Si and B_2O_3 samples irradiated with ^{132}Xe ions with 167 MeV energy

11. Study of theoretical bases of molecular dynamics of B_4C and

BN samples irradiated with ^{132}Xe ions with 167 MeV energy

12. Investigation of thermophysical effects of B_4C, BN, B_6Si and B_2O_3 samples under the influence of neutrons, high-intensity electron flow, gamma rays and fast heavy ions

Research objects;

1**.** Rhombohedral spatial structure (r-B_4C) boron carbide microcrystals with purity 99.9%, specific surface area 28 m^2/g, particle size 1-3 mμ, powder density 1.8 g/cm^3 were used;

2. Hexagonal spatial structure (h-BN) boron nitride microcrystals with 99.8% purity, specific surface area 76-120 m^2/g, particle size 3-8 mμ, powder density 2.29 g/cm^3 were used;

3. Hexagonal spatial structure (h-B_6Si) boron silicate microcrystals with purity 99.5%, specific surface area 68 m^2/g, particle size 40 mμ, powder density 2.43 g/cm^3 were used;

4.Tetragonal spatial structure (t-B_2O_3) boron oxide nano-compound with purity 99.99%, specific surface area 32 m^2/g, particle size 80 nm, powder density 2.6 g/cm^3 was used;

The scientific innovations of the work are as follows: For the first time in the presented dissertation work:

1. The basics of the mechanism of decomposition of water molecules absorbed on the nano-boride oxide layer with fast neutrons are given;

2. Changes in crystal size in nano B_2O_3 crystals under the influence of fast neutron flowes of different intensities have been identified;

3. The mechanism of thermal transitions with fast neutrons of different intensities in nano B_2O_3 crystals has been determined;

4. Vigner's energy kinetics under the influence of fast neutrons in the temperature range $300 \leq T \leq 1300K$ in boron nitride microcrystals was determined;

5. Changes and regularities of lattice parameters in samples under the influence of high-energy electron flow were studied;

6. Changes in thermal conductivity and thermodiffusion in B_4C and B_6Si samples under the influence of high-energy and high-intensity electron flow in the temperature range of $100 \leq T \leq 300K$ were studied;

7. The dynamics of swelling distribution in the surface morphology of samples irradiated with fast ^{132}Xe ions with an energy of 167 MeV was studied;

8. Changes in thermophysical parameters and thermodynamic functions were determined in research samples in the temperature range of $100 \leq T \leq 300K$;

9. Kinetics of molecular dynamics of defects in the crystal structure of research samples under the influence of fast heavy ions was developed on a mathematical basis;

10. The kinetics of thermodynamic functions in the temperature range $300 \leq T \leq 1300K$ of B_4C, BN, B_6Si and B_2O_3 samples irradiated with fast heavy ^{132}Xe ions with energy of 167 MeV was revealed;

11. The nature of color centers formed by gamma rays in B_4C compounds has been studied;

12. The kinetics and depth of the oxidation mechanism were determined in B_4C and B_6Si samples under the influence of gamma irradiation;

13. Element mapping, amorphous mechanism, distance between atoms and changes in structural parameters under the influence of gamma irradiation have been identified;

Practical significance of the work: The practical significance of the dissertation is that the study of dynamics of surface morphology, structural analysis and optical properties of ceramic and oxide compounds of boron chemical element with different energy, thermophysical properties by varying intensity irradiation methods was carried out. In addition to the main part of the dissertation, the structure of the model experiments under the influence of various irradiation on the studied materials, Raman and IR spectroscopic analysis, Atomic Force Microscopy (AFM) and Scanning Electron Microscope show that boron compounds are sufficiently irradiation-resistant and practically promising in these types of irradiation.

In solving the problems raised in the dissertation, it was determined that the mechanism of surface degradation in B_4C, BN and B_6Si compounds under different irradiation conditions, depending on the temperature, is weak. Accurate thermophysical kinetics for oxidation kinetics and oxide layer thickness in ceramic compounds

have been determined depending on the wide temperature range. Based on all determined thermophysical values, the ability of samples to work in the practical temperature range allows us to predict the exact date of the efficiency coefficient and modernization period. The results provide a basis for predicting the oxidation mechanism, boron-based detector and average service life of absorbent materials for simultaneous irradiation conditions in nuclear technology.

The main provisions of the defense:

1. The nature of structural defects in research objects and the mechanism of defect formation by different methods;
2. Regularities of change of thermophysical parameters at low temperatures under different irradiation conditions;
3. Crystal size change under the influence of irradiation;
4. The nature of Vigner energy and temperature-dependent kinetics;
5. Study of the mechanism of "swellings" in surface morphology during rapid irirradiation with heavy ions;
6. Molecular dynamics of defects on a mathematical basis;
7. Study of the nature of color centers formed by gamma rays;
8. High-temperature oxidation mechanism with gamma rays and oxide layer thickness;
9. Changes in the mechanism of amorphization under the influence of irradiation have been studied.

Approbation of the work:

The materials of the dissertation were presented and discussed at international and domestic conferences. The results obtained have been discussed in international, domestic and other scientific seminars and conferences in different years with the following reports.

1. M.N. Mirzayev, B.A. Skuratov, E. Demir, N.V. Tiep, E.B. Asgerov, S.H. Jabarov, Kh.F.Mammadov, R.N. Mehdiyeva, A.B. Tuğrul, R.G. Garibov, Study of atom dynamics of the (SS GRADE 321)+B_4C+Al_2O_3 compounds under heavy ion irradiation, Radiation Processes and Their Applications, Baku, Azerbaijan, 13-15 November 2018.

2. M.N. Mirzayev, Kh.F. Mammadov, R.N. Mehdiyeva, S.H. Jabarov, E.B. Asgerov, S.M. Akberova, Chances crystal structure of silicon hexaboride irradiated under gamma ray, 18th International Conference on Radiation Physics and Chemistry of Condensed Matter, EFRE – 2018, September 16-22, Tomsk, Russia, 2018. p.528

3. M.N. Mirzayev, Kh.F. Mammadov, R.N. Mehdiyeva, Microstructural, macroscopic length and lattice parameters changes in gamma-irradiated boron carbide. Modern Trends in Condensed Matter Physics, MTCMP – 2018, September 24-26, Baku, Azerbaijan, 2018. p.118

4. M.N. Mirzayev, E. Demir, D.M. Mirzayeva, B. Abdurakhimov, Assessment of oxidation kinetics of boron carbide under gamma irradiation conditions, The Ninth International Conference "Modern Problems of Nuclear Physics and Nuclear Technologies", September 24-27, Tashkent, Uzbekistan, 2019, pp 262.

5. M.N. Mirzayev, Kh.F. Mammadov, D.M. Mirzayeva, V.A. Skuratov, E. Demir, E. Popov, Defects processes and formation of Wigner enthalpy in boron carbide under neutron irradiation, 7th International Conference on Energy Fluxes and Radiation Effects, EFRE – 2020, September 14-25, Tomsk, Russia, 2020. P.459

6. M.N. Mirzayev, E. Popov, A.S. Doroshkevich, E. Demir, F. Mamedov, I.G. Genov, R.N. Mehdiyeva, Z.A. Sharipov, Thermic and electrical analogy of B_4C and BN under different irradiation, Радиационная Физика Твёрдого Тела, Севастополь, 05-10 июля 2021 г. p.313-315.

7. Kh.F. Mammadov, M.N. Mirzayev, R. Garibov, G. Allahverdiyev, Study of the processes of changing the crystal structure of boron carbide after the destruction of a nuclear reactor as a result of earthquake, Natural disasters and human life safety, 2017, Baku, Azerbaijan

8. A. Dalcalı, I. Koçak, M.N. Mirzayev, E. Demir, V. Uglov, V. Shymanski, B. Büyük, Boron mine and assesment of regional development (3rd International Regional Development and The Role of Universities Symposium) November 21-22, 2019, Bandırma, Balıkesir, Turkey

9. E.P. Popov, A.N. Chernikov, A.I. Beskrovnyi, J. Waliszewski, M.N. Mirzayev, Cryostat for cooling samples in the study of low-temperature structural and magnetic phase transitions by neutron diffraction, Journal of Physics: Conference Series 1492 (1), 012054, 2020.

10. Demir, M.N. Mirzayev, E. Popov, D.M. Mirzayeva, An experimental study on thermal properties of boron based compounds under ionization irradiation, Second International Scientific Conference of Young Scientists on "Multidisciplinary approaches in solving modern problems of fundamental and applied sciences (Natural sciences), 03–06 March 2020, Baku, Azerbaijan.

11. S. Makatsaria, L. Chkhartishvili, M. Mirzayev, N. Barbakadze, O. Tsagareishvili, I. Jinikashvili, R. Chedia, Nanopowder h-BN:Fe(Fe_3O_4) as ^{10}B delivery agent in BNCT, ISBB2022, the 21st International Symposium on Boron, Borides and related materials related, from 5 to 9 September 2022, Paris, France.

12. N. Gogolidze, L. Chkhartishvili, M. Mirzayev, N. Barbakadze, O. Tsagareishvili, M. Buzariashvili, O. Lekasvili, R.Chedia, Preparation of sandwich-like B_4C/W neutron-shield materials, ISBB2022, the 21st International Symposium on Boron, Borides and related materials related, from 5 to 9 September 2022, Paris, France.

Publications: The main content of the dissertation is reflected in 16 articles and 8 theses published in the world's leading scientific journals, as well as 5 articles and 4 theses published in the country. The main results of the dissertation were published in 30 scientific works, including 21 articles and 12 theses.

The structure and scope of the dissertation. The dissertation consists of an introduction, seven chapters, the conclusion and the reference. The submitted work consists of 333 pages, 145 figures and 42 tables and 413515 symbols. The number of used literature is 308, including the author's articles.

BRIEF CONTENT OF THE DISSERTATION WORK

The introduction part consists of the substantiation and relevance of the dissertation, multifunctional features of research materials, technological and practical significance and the main

provisions of the topic to be defended.

In the first chapter of the dissertation the crystal structure of ceramic compounds of boron, the mechanism of formation, obtaining binary and composite structure of different composition, a brief overview of different spatial modifications depending on the atomic concentration of boron and experimental experiments with different sources of irradiation, regularities of structural distribution of kinetic energy of ions of different intensities transmitted to the atoms of boron compounds are studied.

In the second chapter of the dissertation provides detailed information the density of nano and micro states of samples selected for research, degree of purity, particle size, specific surface area, mass ratio in a crystalline compound, melting and evaporation temperature, the chemical hardness of the samples selected for research and various irirradiation methods. Infrared, Raman spectroscopic and atomic force microscopy analysis methods were presented in order to study structural analysis, determination of spatial groups, change in the distance between atoms in a crystal lattice, lattice parameters, surface morphology, nature of surface and volume defects, the mechanism of swelling and amorphization formed on the surface after irirradiation.

In the third chapter of the dissertation, the compounds B_4C, B_6Si, BN and B_2O_3 are in impulse mode, after irirradiation with E <1 MeV energy, fast neutrons at 4.0×10^{12} n/(cm²×sec), 8.0×10^{12} n/(cm²×sec), 1.37×10^{13} n/(cm²×sec), 4.0×10^{14} n/(cm²×sec), 1.0×10^{15} n/(cm²×sec) intensity, the possible elastic and inelastic interactions of the research materials with the atomic nuclei, the possibility of the interaction of high-intensity neutron flowes with atoms located at the nodes of the lattice in the mechanism of defect formation have been widely studied. The diffraction spectrum of B_2O_3 nano crystal studied by X-ray structural analysis corresponds to the C*mc*2 spatial group, β-B_2O_3 modification with lattice parameters a = 0.4613 nm, b = 0.7803 nm and c = 0.4129 nm, and it was determined that the nano B_2O_3 sample is 90 nm. Figure 1 shows small and large vibration modes of BO_3, BO_4, B(OH) and OH groups up to 4000 cm^{-1} frequency in different parts of the nano boron oxide compound. Modes 630 cm^{-1} and 700 cm^{-1} B-O-B of the first functional groups included in the large

vibration group are used for bending oscillations of BO_3 borate groups at different angles, frequencies included in the second group are 880 cm^{-1}, 920 cm^{-1}, 930 cm^{-1}, and 1195 cm^{-1} corresponds to BO_4, B-O tension oscillations. 1027 cm^{-1}, 1045 cm^{-1}, 1057 sm^{-1}, 1066 cm^{-1} və 1079 cm^{-1} characterize the B-O stretched oscillations of the di-borate and tetra borate BO_4 group. Modes of 1253 cm^{-1} and 1470 cm^{-1} BO_{sim} B-O_{sim} symmetrically stretched pyro and ortho borate groups were not observed. The functional groups observed at low frequencies of 2263 cm^{-1}, 2369 cm^{-1}, and 2519 cm^{-1} coincide with the B- (OH) oscillation modes. The effect of neutron irradiation increases the intensity of motion modes and leads to the formation of new functional groups 2900 cm^{-1}, 2989 cm^{-1}, 3676 cm^{-1}, and 3735 cm^{-1}. Starting from the value of intensity 1.3×10^{13} n/cm², it is possible to clearly observe the functional groups of OH. Under the influence of neutron flow, various chemical and physical transformations occur in the structure of nano-crystalline B_2O_3 compounds as a result of elastic scattering, inelasticity, (n, 2n), (n, γ) and irradiation trapping in the samples. Namely, the amount of energy transferred to the system increases linearly as a result of the process of inter-nuclear interactions under the influence of neutron flow, transformations with the B^{10} isotope, and elastic scattering. The increasing amount of energy creates free, broken down phases of the hydrate and hydroxide group, so that the effects of the free groups can be clearly seen in the spectrum. Depending on the intensity of the irradiation, the new effects are parallel to the absorbed energy and increase. Intensity of neutron irradiation from 1.3×10^{13} n/cm² to 1.0×10^{15} n/cm² indicates that the hydroxide group remains anionic and cationic in the crystal structure.

Studies have shown that nano B_2O_3 samples with high chemical activity can retain the irradiation-resistant OH-hydroxide group. In addition to the interaction with the B^{10} isotope, the release of 2.4 MeV of energy and the energy loss of the neutron flow during the interaction have a maximum value for the hydrogen nucleus and water molecules. The energy of the neutron is transferred to the hydrogen and water molecules in the $B(OH)_3$ and HOBO compounds formed in the B_2O_3 structure by the following mechanism, and the decomposition process takes place.

$$B_2O_3 + H_2O \xrightarrow{Neutron\ flux} O = B - O - H \rightarrow H^+ + |BO|_3^-$$

$$B_2O_3 + H_2O \xrightarrow{Neutron\ flux} O = B - O - H \rightarrow |BO|_4^+ + OH^-$$

$$B_2O_3 + H_2O \xrightarrow{Neutron\ flux} HO - B = [O - H]_2 \rightarrow B[OH]^+ + OH^-$$

Some of the H^+ atoms formed are captured by active centers formed by the neutron flow. On the other hand, H^+ atoms combine to form molecular H_2 and separate as a decomposition product.

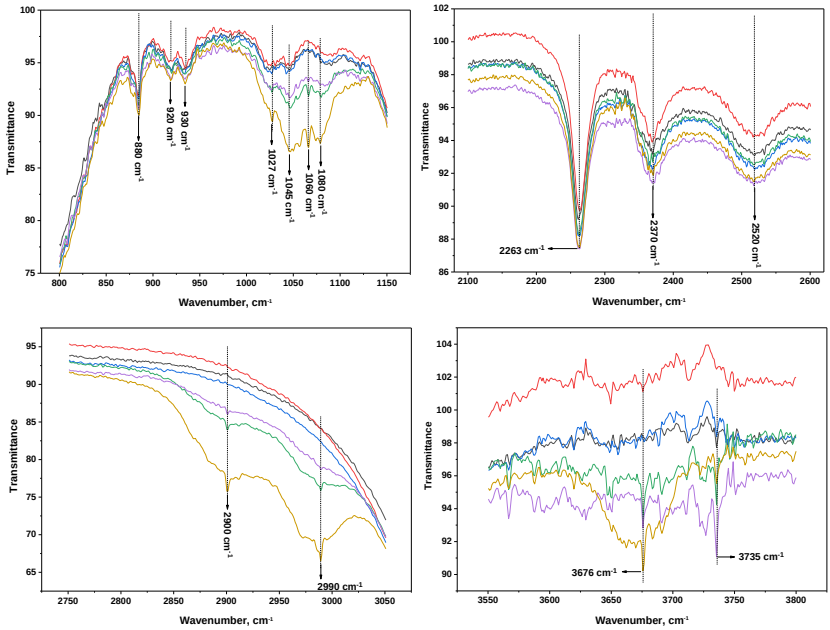

Figure 1. Infrared spectra of nano-crystalline B_2O_3 samples irradiated with fast neutrons at room temperature at initial and different intensities. (black-primary, red-4.0×10^{12} n/cm², blue-8.0×10^{12} n/cm², green-1.3×10^{13}, pink-4.0×10^{14} n/cm² and yellow -1.0×10^{15} n/cm²).

After neutron irirradiation, the maximum value of the force constant of the interatomic chemical bond in the existing new and emerging groups was determined for the OH functional groups, and the lowest value for the BO_4 stretched groups. Under the influence of

high-intensity neutron flow, p-electron of a boron atom is transferred to an oxygen atom during the formation of a new B-O covalent chemical bond and the chain process. Boron atoms undergo an oxidation reaction with electron transfer, and their reduction reaction properties predominate. The formation of B- (OH) chemical bonds in the structure is due to the transfer of electrons to the B atom by functional groups (anions [OH] ¯) formed as a result of neutron irradiation. In Figure 2, Raman peaks of nano B_2O_3 compounds at frequencies 207 cm^{-1}, 498 cm^{-1}, 527 cm^{-1}, 883 cm^{-1}, 921 cm^{-1} and 1165 cm^{-1}were observed under the influence of neutron flow of different intensity at room temperature.

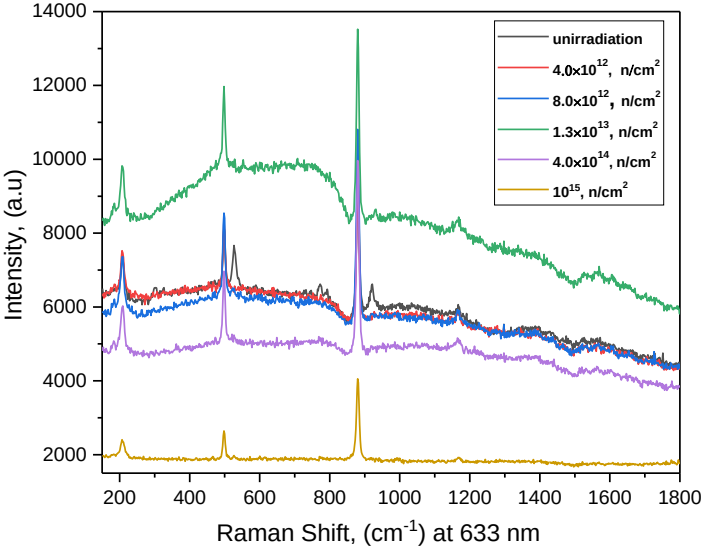

Figure 2. Raman spectra of nano B_2O_3 compounds under the influence of neutron flowes of different intensities.

Known frequencies or chemical bonds characterize 883 cm^{-1}, 921 cm^{-1} and 1165 cm^{-1} boron acid and B-O bonds. The peaks marked 498 cm^{-1} and 1165 cm^{-1} indicate the presence of B-O-B corresponding oscillations of the B_2O_3 phase. Depending on the intensity of the neutron in the Raman spectra, it is clear that an additional group of oscillations occurs at 207 cm^{-1}. In addition, changes in the thermal flow function, heat capacity and thermodynamic functions of boron

compounds irradiated with fast neutrons at different intensities were studied. The kinetics of the heat flow function, 4.0×10^{12} n/cm², 8.0×10^{12} n/cm², 1.3×10^{13} n/cm², 4.0×10^{14} n/cm² and 1.0×10^{15} n/cm² of irradiated B_2O_3 sample in the temperature range $100\leq T\leq800$K can be divided into three parts.

- $422\leq T\leq443$K decomposition reaction of HBO_2 and $B(OH)_3$samples
- Decomposition reaction of $456\leq T\leq600$K H_2O and OH groups
- $T\geq600$K constant temperature range or stable region

Double endo effects occur up to a temperature of 443K, after 456 K the heating rate is more complex or very peak. The final process is the transition to a constant temperature range. Given that in the B_2O_3 sample, under the conditions of synthesis, depending on the storage conditions, various "thermochemical" chemical reactions with water molecules take place in the open air (according to the following transition mechanisms).

$$B_2O_3 + H_2O \rightarrow 2HBO_2$$
$$B_2O_3 + 3H_2O \rightarrow 2B(OH)_3$$
$$\frac{1}{2}B_2O_3 + \frac{1}{4}H_2O \rightarrow \frac{1}{4}H_2B_4O_7$$

As a result of the influence of temperature, the following decomposition reactions occur.

$$2H_3BO_3 \rightarrow 2HBO_2 + 2H_2O\uparrow$$
$$2HBO_2 \rightarrow B_2O_3 + H_2O\uparrow$$
$$\frac{1}{4}H_2B_4O_7 \rightarrow \frac{1}{2}B_2O_3 + \frac{1}{4}H_2O\uparrow$$
$$HBO_2 \rightarrow \frac{1}{4}H_2B_4O_7 + \frac{1}{4}H_2O\uparrow$$
$$2B(OH)_3 \rightarrow B_2O_3 + 3H_2O\uparrow$$

It is clear that the mechanism of the hydration and dehydration reactions that occur in samples of boron oxide irradiated under the influence of non-irradiated and neutron flowes is even more complex. In the samples, the doublet effects show the decomposition reaction of $HBO_2\rightarrow B_2O_3$ at 422 K and the decomposition reaction (transition) of boron acid $B(OH)_3 \rightarrow B_2O_3$ at 438 K. The main decomposition products are complex reactions involving the separation of the OH group and structural water. The fields of doublet effects that

characterize the decomposition reaction in nano boron oxide samples increase depending on the neutron intensity. The intensity of the peak formed in the non-irradiated sample is 1.614 times smaller than in the irradiated samples at different absorption doses. An increase in the field of effect and neutron intensity indicates that a large amount of energy is required to complete the kinetic process. After each neutron intensity, the OH group and radicals in the free state increase, and under the influence of temperature, the reaction products break down in a faster phase. Depending on the neutron flow intensity in the samples, the change in energy required for the decomposition reaction in the doublet effects in the temperature range $422 \leq T \leq 438K$ and $438 \leq T \leq 443K$ is given in Figure 3.

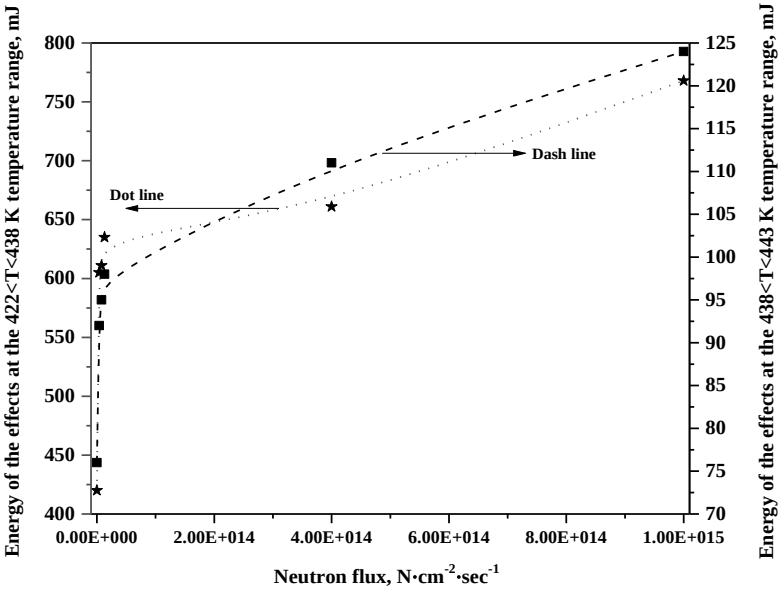

Figure 3. Energy effects on B_2O_3 nano crystal, non-irradiated and irradiated with neutron flow of varying intensity in the temperature range $422 \leq T \leq 438K$ and $438 \leq T \leq 443K$.

It is clear that depending on the intensity of the neutron flow, the conversion energies in the range of 4.0×10^{12} n/cm² $\leq n \leq 1.3 \times 10^{13}$ n/cm² are close to each other. However, starting from the intensity $n \geq 4.0 \times 10^{14}$ n/cm², the conversion energy line increases. Once again, it

is clear that in a transformation reaction with a complex mechanism, the neutron flow increases the decomposition of water molecules in the free state and the number of hydroxide groups. At high absorption doses, the decomposition reaction of water vapor and OH groups is not completed and the energy change is stable. Figure 4 shows the calorimetric spectra of the decomposition reactions of different groups with more series and different types of interactions in the samples, depending on the neutron intensity in the temperature range 450≤T≤580K.

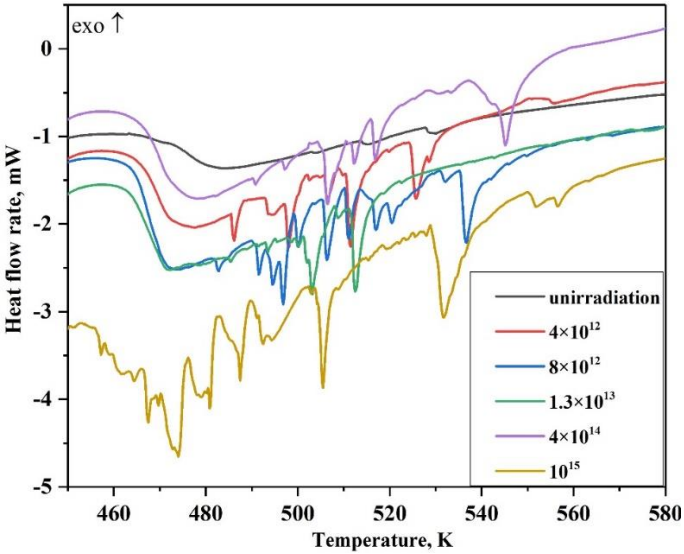

Figure 4. Effects of heat flow on B_2O_3 sample non-irradiated and irradiated with neutron flow of varying intensity in the temperature range 450≤T≤580 K.

It is clear from Figure 4 that the high neutron flow increases the number of decay centers and is a series of transformation reactions that occur by the mechanism $B_2O_3 \rightarrow H_3BO_3$ in a compound of nano boron oxide with high chemical activity in the temperature range 450≤T≤580K.

$$2H_3BO_3 \rightarrow 2HBO_2 + 2H_2O \uparrow$$
$$2HBO_2 \rightarrow B_2O_3 + H_2O \uparrow$$

As the neutron intensity increases, new endo centers are formed. Each new endo formed under the influence of neutron

irradiation shows experimentally the phase of decomposition of the hydrate and hydroxide group under the influence of central temperature. In the non-irradiated sample, the endo effects corresponding to the central peak temperatures of 503K, 515K, and 530K increase even more after irirradiation. Depending on the irradiation dose, the temperature changes of the endo effects to the small values of 457K and large 556K confirm the above ideas. The temperature dependence of the heat capacity shows that the heat capacity of the samples at 100 K varies from 0.310 J/K×g for the non-irradiated sample to 0.315 J/K×g, 0.317 J/K×g, 0.322 J/K×g, 0.326 J/K×g, and 0.333 J/K×g after irirradiation with neutron flow of different intensities (4.0×10^{12} n/cm², 8.0×10^{12} n/cm², 1.3×10^{13} n/cm², 4.0×10^{14} n/cm² və 1.0×10^{15} n/cm²). However, at a temperature of 600 K, the heat capacity of the samples increases to 0.458 J/K×g for the non-irradiated sample and to 0.483 J/K×g, 0.488 J/K×g, 0.497 J/K×g, 0.501 J/K×g və 0.513 J/K×g for the samples irradiated with neutron flow of different intensities.

The peaks of the existing plane diffraction for boron nitride in the chapter are (002), (100), (101), (102), (004) and (110) planes of the hexagonal phase of the boron, space group: P-6, a = 2.5092 nm ; c = 6.6762 nm; $\alpha = 90^{\circ}$; $\gamma = 120^{\circ}$ was determined. The boron nitride sample was investigated under a stream of inert Ar gas with main peak centers and a heating rate of 5˚C/min in the temperature range $400\leq T\leq1300$K. The heat flow function does not change until the temperature reaches 400 K, however, the kinetics of the released Wiegner energy covers a region and is defined as "Wiegner energy" in the temperature range $770\leq T\leq1220$K. The results of DSC analyzes (including oxidation reactions) show that the crystal structure of boron nitride is characterized by the formation of characteristic natural defects in volume or surface due to synthesis conditions or other effects. Depending on the mechanism of formation of defects and their migration, Wigner effects occur in different temperature ranges. Experimental results show that as the value of the irradiation dose increases, the amount of energy stored in the boron nitride compound increases. Figure 5 shows the dependence of the energy stored in the BN compound on different neutron irradiation. As a result of elastic

scattering and irradiation trapping of neutron flow from boron and nitrogen nuclei, various defect centers are formed in the crystal structure. In the process of neutron flow interaction with the B^{10} radioisotope, $_2He^4$ ion along three energy lines (1.47 MeV, 1.78 MeV və 2.05 MeV), $_3Li^7$ ion two energy lines, 0.48 MeV gamma rays, $_1H^3$ ion two energy lines (2.72 MeV and 191 keV) and 573 keV energy deuterium form large defect centers in the BN structure.

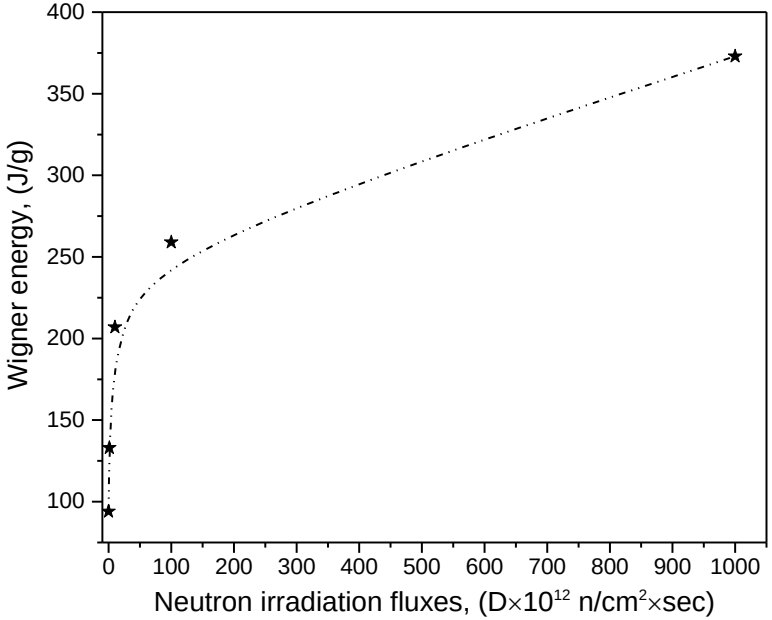

Figure 5. Change of stored energy graph based on neutron flow for BN sample.

In addition, the interaction of neutron flowes with the 14N nucleus to obtain 40 keV 14C and 580 keV 1H proton isotopes, in turn, creates new types of defects. Also, as the neutron intensity increases, the amount of energy transferred to the crystal structure increases. Large number of defect centers create a large accumulation of energy. In non-irradiated samples, the value of energy stored at neutron intensities ranging from 8.0×10^{12} n/cm² to 4.0×10^{14} n/cm² increases slightly from 133.106 J/g to 259.364 J/g, while the amount of energy accumulated due to the main defects is 94.49 J/g. However, the

maximum neutron irradiation of 1.0×10^{15} n/cm² indicates that the value of the stored energy increases faster and reaches 373,609 J/g. This shows once again experimentally that a high irradiation dose is equivalent to a high Wigner energy.

In the **fourth** chapter of the dissertation, research samples were irradiated at room temperature with 2.5 MeV energy, high intensity 4.16×10^{16} 1/cm^2, 1.20×10^{17} 1/cm^2 and 1.03×10^{18} 1/cm^2 electron flow. Theoretical and experimental bases of possible elastic and inelastic interaction of electron flow with atoms located in the structural structure of research materials were analyzed and the mechanism of energy transferred to crystalline volume was determined. The study of irradiation effects on the structure of irradiated samples, changes in the heat flow function of samples in the temperature range 100<T<300 K, determination of heat capacity and other thermophysical parameters are given.

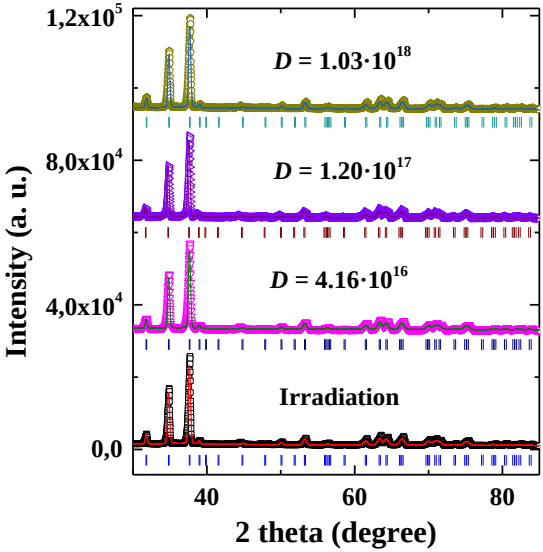

Figure 6. X-ray diffraction spectra of B_4C microcrystals obtained after irradiation with electron flow at room temperature, normal atmospheric pressure and different intensities.

Figure 6 shows the X-ray diffraction spectra of a microcrystalline B_4C sample obtained after irirradiation with electron

beam at room temperature and at different doses. The analysis of the spectra showed that under normal conditions and at room temperature, boron carbide has a rhombohedric symmetrical crystal structure of the R-3m space group. Lattice parameters were defined as: a = 5.62922 Å and c = 12.13944 Å, which is consistent with previous research results. Analysis of X-ray diffraction spectra of non-irradiated samples, irradiated samples at doses of 4.16×10^{16} 1/cm^2, 1.20×10^{17} 1/cm^2 və 1.03×10^{18} 1/cm^2 showed that no phase transitions occur in the crystal structure of the B_4C compound in the specified intensity range. All spectra correspond to the R-3m spatial group and rhombohedral symmetry.

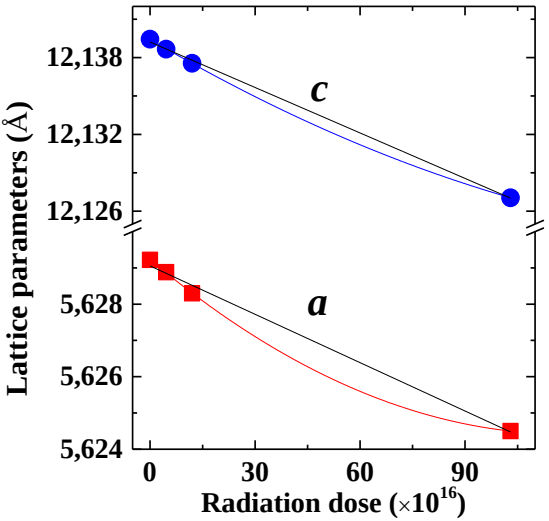

Figure 7. Change of lattice parameters after irradiation of boron carbide sample with electron flow at room temperature.

Only a certain shift of diffraction maxima along the abscissa axis and a change in intensity were observed, which corresponds to a partial change in lattice parameters and atomic coordinates under the influence of electron irradiation. In Figure 7, the change in lattice parameters depending on the irradiation intensity shows that as the irradiation intensity increases, the values of lattice parameters a and c, similar to the linear (black lines) function, decrease by the law $a_i =$

$a_0 - k_i D$. For parameter a: $a = 5.63 - 4.44 \cdot 10^{-5} \cdot D \cdot 10^{16}$, and for parameter c: $c = 12.14 - 1.18 \cdot 10^{-4} \cdot D \cdot 10^{16}$were obtained. As the value of the irradiation intensity increases, a decrease in the values of the lattice parameters is observed, which can be explained as the replacement of bonds as a result of recombination of defects inside the crystal under the influence of an electron flow.

Table 1. Atomic coordinates of a boron carbide sample irradiated with a stream of electrons of different intensities.

Irradiation				4.16×10^{16} 1/cm^2			
Atom	*x*	*y*	*z*	Atom	*x*	*y*	*z*
B1	0.441	0.558	0.049	B1	0.441	0.557	0.049
C11	0.441	0.558	0.049	C11	0.441	0.557	0.049
B2	0.504	0.495	0.19117	B2	0.504	0.495	0.1911
B3	0	0	0	B3	0	0	0
C1	0	0	0.12339	C1	0	0	0.1232
B11	0	0	0.05628	B11	0	0	0.0549
1.20×10^{17} 1/cm^2				1.03×10^{18} 1/cm^2			
Atom	*x*	*y*	*z*	Atom	*x*	*y*	*z*
B1	0.441	0.557	0.04399	B1	0.441	0.557	0.0435
C11	0.441	0.557	0.04399	C11	0.441	0.557	0.0435
B2	0.504	0.494	0.19085	B2	0.504	0.493	0.1907
B3	0	0	0	B3	0	0	0
C1	0	0	0.12322	C1	0	0	0.12312
B11	0	0	0.053	B11	0	0	0.053

As the irradiation dose of boron carbide irradiated with gamma quanta increases, the values of the lattice parameters decrease, and after a certain dose, the interatomic bonds are broken and the transition from the crystalline phase to the amorphous phase occurs. However, studies have shown that electron flow have a different effect than gamma rays. On the contrary, there is a decrease in the values of the lattice parameters. This is due to the fact that electron beams create a mechanism for changing interactions between atoms (colored lines), recombination of existing defects in the crystal structure. In Figure 7, the nonlinear dependences of the lattice parameters show that a certain value of the electron beam can settle, and at that point all the defects in the crystal structure will recombine and recrystallize. Before and

after irirradiation, the boron carbide sample shows the coordinates of the atoms in different crystallographic positions. From the results obtained, it is clear that some atoms cannot be affected by electron beams because they are in their ideal positions.

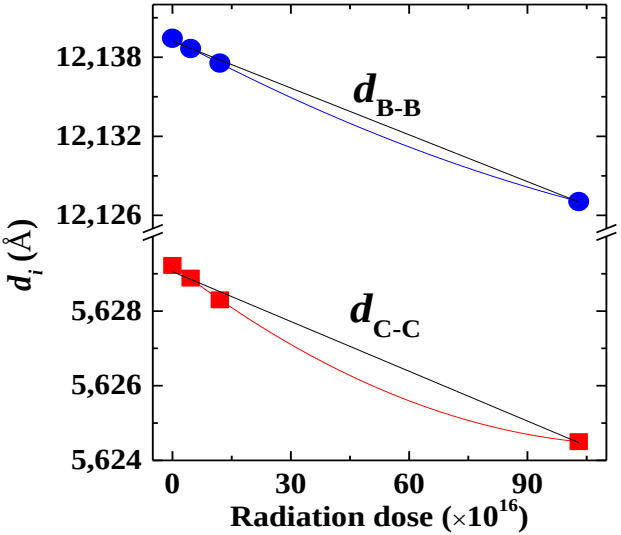

Figure 8. Dependence of distance between atoms on irradiation intensity.

However, atoms that have shifted somewhat from their ideal centers change their coordinates to some extent under the influence of electron beams, which ultimately leads to a change in the distances between the atoms and the corresponding lattice parameters. From the dependences obtained for the average values of the interatomic distances, it was determined that just as the values of the lattice parameters depend on the irradiation flow, the values of the interatomic distances decrease as the irradiation intensity increases. As the intensity of irradiation increases, the mean values of the distances between the atoms B - B, B - C and C - C are similar to the linear (black lines) function: decrease occurs with the law $d_i = d_0 - k_i D$ (Figure 8). For B - B atoms: $d_{\mathrm{B-B}} = 5.63 - 4.44 \cdot 10^{-5} \cdot D \cdot 10^{16}$, for B - C atoms: $d_{\mathrm{B-C}} = 5.63 - 4.44 \cdot 10^{-5} \cdot D \cdot 10^{16}$, for the atoms C –C: $d_{\mathrm{C-C}} = 5.63 - 4.44 \cdot 10^{-5} \cdot D \cdot 10^{16}$are obtained.

In the **presented** chapter, raman spectra at different concentrations of boron and carbon atoms in boron carbide compounds have been studied. The research provides more detailed information about the dynamics of the B12, B11C icosahedron, C-B-C and C-B-B chains at different frequencies and the movement of the lattice.

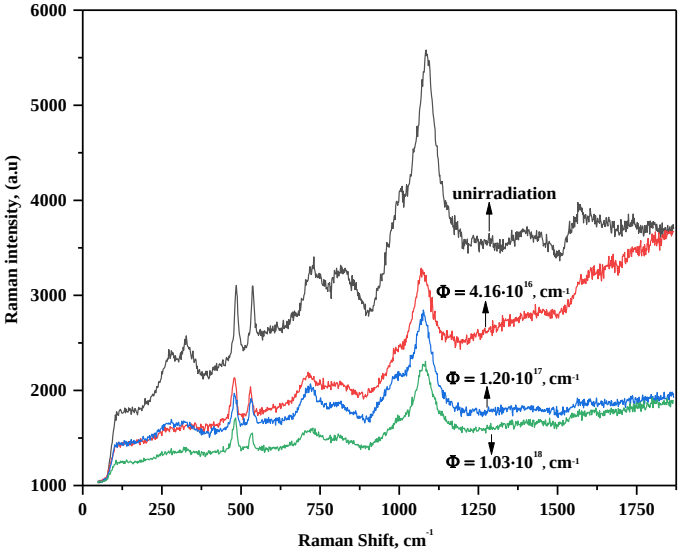

Figure 9. Raman spectra of boron carbide compound non-irradiated and irradiated at different electron intensities

According to the group theory, five of the eleven (11) active Raman modes present in the boron carbide sample formed in the form of a $(B_{12})CBC$ or $(B_{12})CCC$ structure are of the (A_{1g}) and six are of the (E_g) symmetry type. Figure 9 shows the Raman spectra of the boron carbide compound non-irradiated and irradiated at different electron intensities. It has been determined that the non-irradiated boron carbide compound has 11 Raman-active spectra. The spectra of Raman active modes were compared with other structural compounds of the boron ($B_{10.37}C$, $B_{8.52}C$, $B_{7.91}C$, $B_{6.3}C$ and $B_{4.3}C$) and it was determined that the $(B_{12})CBC$ sample we studied had a larger crystalline structure. The results of the structural analysis once again showed that the boron and carbon atoms are in a 6.5: 1 ratio and that

$B_{13}C_2$ is formed in the form of a structure. The diffuse effects were observed in the boron carbide sample at 270, 323, 730, 820, 1007, 1087, 1395 and 1574 cm^{-1} Raman frequencies. The scattered spectra provide more information about the amor phase or partially disturbed crystal structure. Three types of double peaks of 270/323 cm^{-1}, 730/817 cm^{-1} and 1004/1084 cm^{-1} were observed from these Raman spectra. Double peaks are precise modes of the equatorial pentagonal shape of three B-C icosahedrons with A_{1g} symmetry type. The most active phase of B-B Raman modes is 1072-1084 cm^{-1}.

It is clear that B-B oscillation modes are completely disrupted at high electronic flow densities. However, the intense Raman spectra of 485 cm^{-1} and 536 cm^{-1} correspond to the oscillations of the $B_{11}C$ chain structure in the oscillation mode of boron carbide crystals. It is clear from the Raman spectra of the irradiated samples that all the scattered spectra are completely degraded. The structure in the amorphous phase shifts to a higher amorphous phase. The intensity of the intense 485 cm^{-1} and 536 cm^{-1} spectra remains seven times that of the unirradiated sample, and the half-width remains unchanged.

At the same time, in the first study of boron carbide after irirradiation **in the chapter**, the heat flow transfer in the temperature range $100 \geq T \geq 146K$ is smaller, but $146 \geq T \geq 300K$ changes in a more active phase, ie a two-phase heat transfer mechanism occurs. The heat flow kinetics for boron silicate is not divided into regions. However, boron carbide with different atomic concentrations is thermodynamically Gibbs formation energy in the temperature range 10-2000 K is a function of carbon concentration and is known to have thermophysical kinetics for boron silicide compounds. However, for boron silicate compounds, heat transfer and flow change follow the same mechanism. If no phase transition is observed in the kinetics that changes according to the linear law, the mechanism of all thermo-physical processes that take place is based on a specific heat capacity and is interconnected. Figure 10 shows the temperature dependence of the specific heat capacity of different irradiations for samples of boron carbide and boron silicate in the temperature range $100 \leq T \leq 300K$. It was found that, regardless of the irradiation energy and intensity, the kinetic variation of the specific heat capacity of a boron carbide

compound increases by a different mechanism at temperatures T≤146K, and by a faster mechanism at temperatures T≥146K. The obtained experimental results suggest that the transfer of heat flow in the boron carbide sample at lower temperatures occurs by a dual mechanism.

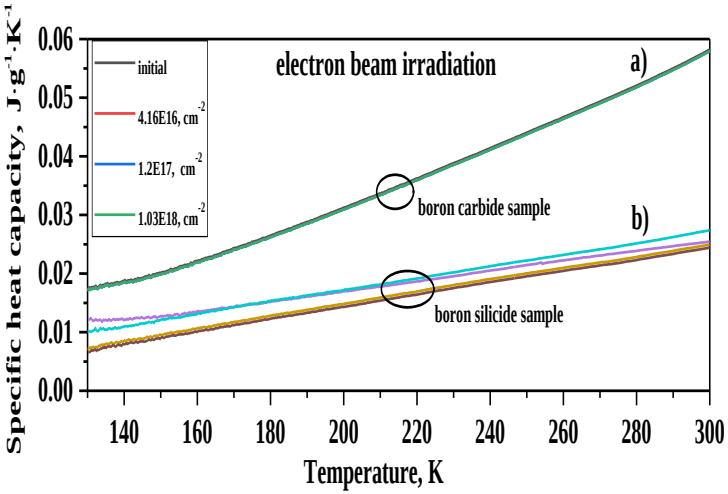

Figure 10. Specific heat capacity of boron carbide and boron silicide samples irradiated at different intensities in the temperature range 100≥T≥300K.

At low temperatures, only the thermal flow transmitted by thermal phonon-phonon interaction is self-contained. The kinetics of the heat flow in the temperature dependence also manifests itself in the temperature dependence of the heat capacity. It is clear from the temperature dependence of the heat capacity that the specific heat capacity of the samples varies around 0.0170-0.0176 J/K×g under the influence of an electron flow of boron carbide samples. The specific heat capacity mechanism for boron silicate samples is also slightly different from that of boron carbide. In the example of boron silicate, the heat transfer mechanism is the line. The transmission of phonon-phonon interactions at low temperatures is only one mechanism. The specific heat capacity of boron silicate samples under the influence of both irirradiations varies around 0.005627-0.0129 J/K×g around a

temperature of 100K. However, this is a very small value compared to the boron carbide sample. Obtaining in both samples in this way is definitely related to their crystal structure and density factor. With increasing density, the interaction of the fanon at lower temperatures in ceramic samples is greater, and this is expressed more by the linear function. It was experimentally observed in samples of boron carbide and boron silicate with different densities. The kinetics of the specific heat capacity for each irradiation are given in Figure 11.

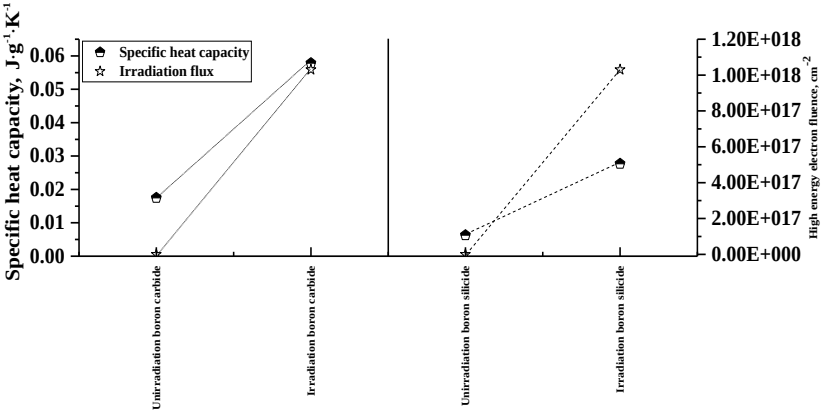

Figure 11. Kinetics of specific heat capacity in the temperature range 100≤T≤300K.

Figure 11 shows the kinetic variation of the specific heat capacity, which shows that the boron carbide compound increases 3.48 times when irradiated with high-energy electrons in the temperature range 100≤T≤300K. For boron silicate, the heat capacity increases by 4.40 times when irradiated with high-energy electrons. This experimentally shows that the value of specific heat capacity in boron silicate samples increases more rapidly. Figure 12 shows the spectra of heat flow function after irirradiation of boron nitride and boron oxide samples with high-energy and intensity electrons in the temperature range 100≤T≤300K. For samples of boron nitride and boron oxide, the kinetics of the heat flow at different electron intensities are divided into two regions.

- The value of the heat flow function decreases with a different mechanism of 125≤T≤150K.

➢ 150≤T≤300K linear mechanism

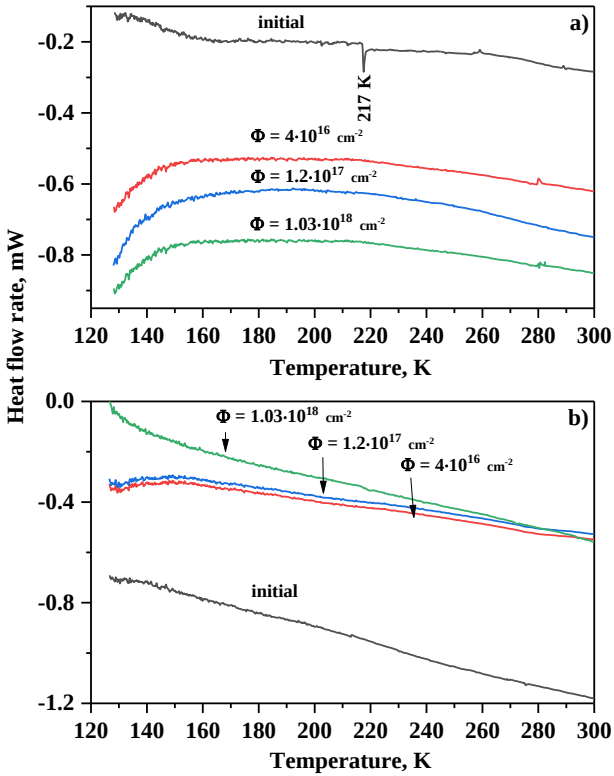

Figure 12. Boron nitride a) and boron oxide b) the heat flow function of the sample after irirradiation at different intensities (4.16×10^{16} $1/cm^2$, 1.20×10^{17} $1/cm^{-2}$ və 1.03×10^{18} $1/cm^2$).

In the example of boron nitride, the mechanism of heat flow propagation under the influence of different electron flowes shows that heat transfer occurs at the same mechanism at all irradiation intensities. After 150K, the heat process is a linear function, and the linear heat flow function is in this temperature range. In addition, the kinetics of the DSC spectra under the influence of an electron stream occur as in the case of boron nitride. Only in the example of unirradiated boron oxide, the function of the heat flow changes linearly, which indicates a linear increase in heat capacity. The

temperature range T≤150K and T≥150K can be defined as a quantum region for the heat flow of a binary mechanism. It was found that the kinetic kinetic variation of the specific heat capacity in the combination of boron nitride and boron oxide, regardless of the electron density, is the same as the thermal flow mechanism. The obtained experimental results give us reason to say that at lower temperatures the transfer of heat flow in the sample of boron nitride occurs by a double mechanism. At low temperatures, the heat flow transmitted by the fanon fanon interaction is binary. The kinetics of the heat flow in the temperature dependence also manifests itself in the temperature dependence of the heat capacity. It is clear from the temperature dependence of the heat capacity that the specific heat capacity of the samples under a temperature of 120K under the influence of electrons of boron nitride samples is very small. It was also found that the mechanism of specific heat capacity for boron oxide samples, regardless of the type of irradiation and irradiation flow, is slightly different from that of boron nitride. In the example of boron oxide, the heat transfer mechanism is the line. The transmission of phonon-phonon interactions at low temperatures is only one mechanism. Boron oxide samples The specific heat capacity of samples under a temperature of 300K under the influence of both irirradiations is a very small value compared to the boron nitride sample. With increasing density, the phonon-phonon interaction at ceramic samples is greater at lower temperatures, and this is expressed more by the linear function.

It was experimentally observed in samples of boron nitride and boron oxide with different densities. This shows experimentally that the value of specific heat capacity in boron oxide samples increases more rapidly. In addition, the change in heat capacity in the more active phase after irirradiation with heavy ions is completely confirmed in all comparative experiments. For a non-irradiated boron carbide sample, the value of thermal conductivity at 120 K was found to be 0.0243 W/cm×K, 0.02420 W/cm×K və 0.02401 W/cm×K, and the value of thermal conductivity for boron carbide after irirradiation at intensities was 0.0247 W/cm×K, 4.16×10^{16} 1/cm^2, 1.20×10^{17} 1/cm^2, 1.03×10^{18} 1/cm^2. After the value of T≤146 K there is a small increase

in the heat flow of boron carbide, the value of thermal conductivity at a temperature of 300 K is equal to 0.0844 W/cm×K, 0.0827 W/cm×K and 0.08 W/cm×K for intensities of 4.16×10^{16} 1/cm^2, 1.20×10^{17} 1/cm^2, 1.03×10^{18} 1/cm^2. In the boron silicate sample, the value of thermal conductivity in the temperature range of 120-300K was determined to vary in the range of 0.015-0.0412 W/cm×K, 0.010-0.0322 W/cm×K, 0.009-0.0335 W/cm×K for 0.0175-0.035 W/cm×K, 4.16×10^{16} 1/cm^2, 1.20×10^{17} 1/cm^2, 1.03×10^{18} 1/cm^2 intensities. The thermal diffusion of boron carbide and boron silicide samples irradiated with high-energy and high-intensity electrons was investigated and it was determined that the change in thermal diffusion in the study samples was very small. The value of thermal diffusion was found to be 0.808-0.794 cm^2/sec, 0.798-0.716 cm^2/sec, 0.767-0.690 cm^2/sec for 0.791-0.806 cm^2/sec, 4.16×10^{16} 1/cm^2, 1.20×10^{17} 1/cm^2, 1.03×10^{18} 1/cm^2 intensities for a boron carbide sample in the 100-300K temperature range. On the other hand, the value of thermal diffusion has a maximum value of 188K at different intensities, which is equal to 0.819-0.810 cm^2/sec. Also, the value of thermal diffusion for a sample of boron silicate in the temperature range of 100-300K was determined to be 0.577-0.579 cm^2/sec, 0.54-0.559 cm^2/sec, 0.44-0.566 cm^2/sec at 0.576-0.591 cm^2/sec, 4.16×10^{16} 1/cm^2, 1.20×10^{17} 1/cm^2, 1.03×10^{18} 1/cm^2 intensities. The decrease in the value of thermal diffusion in the studied temperature range for boron carbide and boron silicate samples was noted, which was explained by the mechanism of phonon-phonon interaction.

In the fifth chapter, research samples B_4C, B_6Si, BN and B_2O_3 were irradiated with heavy ions of 167 MeV energy, ^{132}Xe speed at different intensities of 5.0×10^{12} ion/cm^2, 5.0×10^{13} ion/cm^2 and 3.83×10^{14} ion/cm^2 at room temperature under high vacuum conditions. Mathematical modeling and molecular dynamics of the penetration depth of heavy ions on the surface of research samples were studied, the structural mechanism of surface morphology was studied in detail. Analysis of the function of heat flow, heat capacity kinetics and thermodynamic functions in argon (Ar) medium over a wide temperature range was performed and a comparative analysis was performed for the values of the obtained thermophysical parameters.

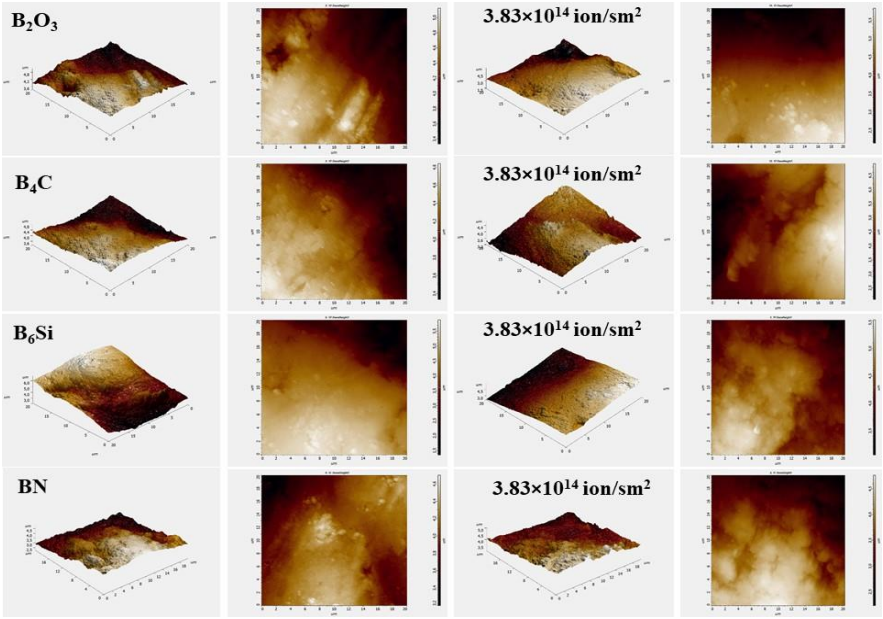

Figure 13. Surface morphology of B_2O_3, B_4C, B_6Si and BN samples irradiated with 167 MeV ^{132}Xe ions at 3.83×10^{14} ion/cm^2 intensity.

Figure 13 shows descriptions of 2D and 3D surface morphology after irirradiation with primary and high-energy ^{132}Xe ions of the B_2O_3, B_4C, B_6Si, and BN compounds. In non-irradiated samples, the maximum size of the microstructure formed on the surface is 4.8±0.5 μm. Also, as seen in the 2D morphology of the original structure, the distribution dynamics of the swellings is weak. After irirradiation with 167 MeV ^{132}Xe ions, the distribution of particles in the microstructure increases according to both the swelling area and the particle size of the swelling. In different places on the surface of the samples, the size of the particles increases after swelling and irirradiation of different sizes in the initial sample. During irirradiation, large swellings are "adsorbed" by small and medium swellings. For multi-layered samples, this process is called "swell interaction effects". As a result, irradiation swellings of different sizes affect the formation of larger affected swellings. The increase in surface swelling in the samples

occurs as a result of thermal processes occurring on the surface. Due to the Johnson approximation, the size of the cylindrical particles is equal to the Johnson parameter. Studies show that the growth rate of swelling on the surface of the samples is 2.2 times higher in non-irradiated samples. The growth rate of the swellings was determined in samples irradiated with 167 MeV ^{132}Xe ions. Ion irradiation is associated with the dislocation of a microstructure that contributes to the formation of swelling on the surface, or "the formation of dislocations in multilayer compounds." Dislocation is formed in the microstructure by two mechanisms (pulsed irradiation and continuous irradiation). Under the influence of the swellings, the process of expanding the parameters of the lattice takes place.

After irradiation of the material with heavy xenon ions, we use XRD experimental methodology to analyze the structural changes in the sample. The whole range of penetration of xenon atoms is seen well enough by XRD, due to the low atomic number of the two elements involved in the material we are studying. Figure 14 shows a shift of X-ray spectra in a B_4C unirradiated and irradiated sample with 167 MeV energy swift heavy $^{132}Xe^{26+}$ ions (SHI). The XRD pattern for the unirradiated sample indicated several peaks of B_4C all assigned to a rhombohedral crystal structure. The rhombohedral crystal structure had a space group of $R\bar{3}m$. The lattice parameters for the unirradiated samples were: a = 5.62922Å and c =12.13944 Å, which correlate with the theoretical values and previous results. In addition, there are B-O covalent bonds on the surface of the unirradiated boron carbide sample, which are characterized by oxygen atoms captured by active boron centers. The capture of oxygen atoms can be shown by the following mechanism.

$$B + O_2 \rightarrow [BO]\bullet + O\bullet$$
$$O\bullet + B \rightarrow [BO]\bullet$$
$$[BO]\bullet + O_2 \rightarrow [BO_2]\bullet + O\bullet$$

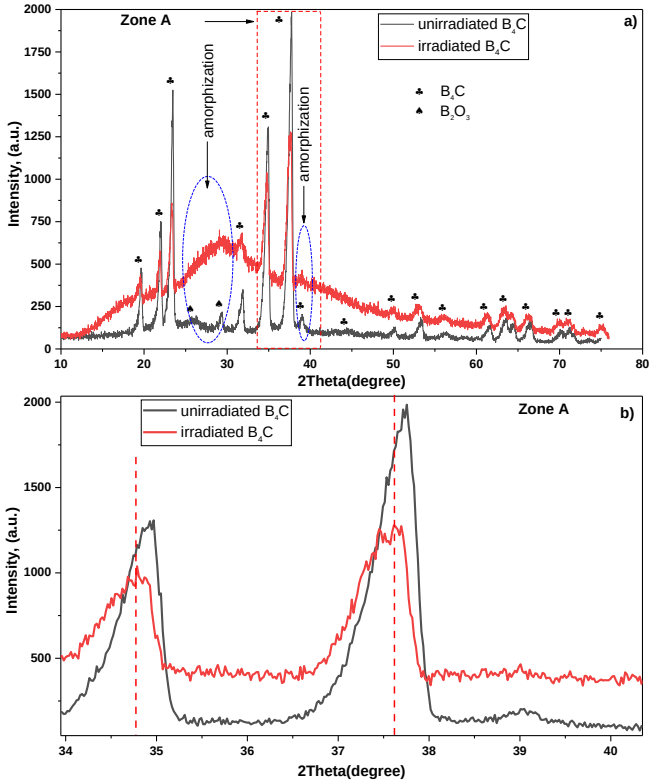

Figure 1. X-ray diffraction of unirradiated (black line) and irradiated boron carbide (red line) at $^{132}Xe^{26+}$ ion 3.83×10^{14} ion/cm^2.

After irradiating the B_4C samples with Xe ions at a fluence of 3.83×10^{14} ion/cm^2, the crystal structure of the samples was observed to change. The lattice parameters of the irradiated samples were obtained as a= 5.65747 Å and c=12.19866 Å. The change in the lattice parameter when compared to the unirradiated samples indicates the partial lattice damage introduce by the SHI irradiation. That is, the irradiated lead to peak broadening and the disappearance of the peaks around the 2-theta position of 26° and 29° (Figure 14b). The 2-theta position of 26° and 29° the disappearing peaks are weakly interacting B-O chemical bonds are degraded under the influence of SHI. A slight peak shift towards the lower theta value (x-axis) was also observed.

The peak broadening observed can be attributed to the partial amorphization of the B_4C.

While the change in the peak position can be possibly due to the lattice disorder (lattice expansion) in the crystal structure and the stress introduced by the SHI irradiation (Figure 14b – Zone A). Peak displacement and decrease in intensity are characterized by the deviation of atoms from the coordinates of the crystal lattice (formation of defect cascade) and the degradation or amorphization of the crystal structure under the influence of high-energy ion streams. In Table 1 showed the crystallite size of unirradiated and irradiated boron carbide sample under 167 MeV energy swift heavy $^{132}Xe^{26+}$ion at 3.83×10^{14} ion/cm^2.

Table 2. Crystallite size of unirradiated and irradiated boron carbide sample under 167 MeV energy swift heavy $^{132}Xe^{26+}$ion at 3.83×10^{14} ion/cm^2.

K	*λ(Å)*	*PP*	*PP*	*FHWH*	*FHWH* $^{132}Xe^{26+}$	*L (nm)*	$^{132}Xe^{26+}$*L (nm)*
0.94	*1.54178*	*19.61*	*←19.51*	*0.31*	*0.42 ↑*	*26.78*	*19.84↓*
		21.97	*←21.86*	*0.33*	*0.37 ↑*	*25.45*	*22.56 ↓*
		23.4	*←23.3*	*0.34*	*0.39 ↑*	*24.82*	*21.56 ↓*
		29.29	-	*0.39*	-	*21.86*	-
		31.77	*←31.49*	*0.51*	*1.98 ↑*	*17.02*	*4.36 ↓*
		34.82	*←34.69*	*0.49*	*0.52 ↑*	*17.92*	*16.76 ↓*
		37.63	*←37.5*	*0.51*	*0.56 ↑*	*17.3*	*15.65 ↓*
		38.0	-	*0.59*	-	*14.89*	-
		50.05	-	*0.76*	-	*12.1*	-
		53.25	*←53.02*	*0.79*	*1.01 ↑*	*11.74*	*9.2 ↓*
		61.51	*←61.3*	*0.81*	*0.63 ↓*	*11.94*	*15.3 ↑*
		63.48	*←63.33*	*1.03*	*1.54 ↑*	*9.5*	*6.34 ↓*
		66.38	*←66.21*	*1.04*	*1.06 ↑*	*9.51*	*9.35 ↓*

From Table 2 shift of peak, disappearing of peaks, full width half-maximum expansion and decrease of crystallite size in irradiated

boron carbide are distributed in the formation of small nano crystal centers because of the high kinetic energy transmitted by the SHI of the crystal. The value of crystallite size increases only at the boron carbide peak, which corresponds to 2-theta position of 61.3°. It is believed that a small amount of new B-C icosahedron is formed as a result of the SHI effect. Reduced grain size with the increasing fluence should improve the sintering properties of the materials that would be used in natural sintering in thermonuclear reactors. The additional fragmentation introduced by the irradiating ions should further ease this sintering process. The XRD pattern indicated that there was partial amorphization in the B_4C crystal structure with parts of the B_4C structure still intact. This indicated that the B_4C material has the ability to retain is crystal structure during swift heavy ion irradiation and the ionization process.

This ability to resist severer damage is useful when considering the ability of candidates to protect plasma from contamination after secondary ionization. Also, from XRD is seen an increase in the number of volumetric defects after irradiation. The positron lifetime (τ) in a growing vacancy cluster was calculated and the defect behavior when B_4C was implanted with hydrogen and helium atoms was studied. There were explore two configurations of this material - $B_{11}C_p$-CBC and B_{12}-CCC, where C_p means C is in polar position in a B-icosahedron. Taking into account the data from the XRD, the lattice parameters in particular, it can be assumed that the material is more likely to be in $B_{11}C$-CBC form. The results are presented in Table 3. The results from the τ calculation (for a perfect lattice on B_4C) are in good agreement with τ_2 that was reported, where the τ_2 value "cannot attribute to cavities and grain boundaries", which we interpret as not to be due to those cavities and grain boundaries. This value can be considered as coming from annihilation of the positron in areas outside the icosahedrons, where a sufficiently low electron density is expected. After irradiation with ions (H/He) or neutrons, defects of vacancy cluster type are expected to be produced. Here we numerically model such vacancy clusters and the values in Table 3

give the dependence of τ on the increase in vacancy volumes and implanted H/He atoms in them.

Table 3. The calculated values for τ in a growing cluster of point defects and hydrogen and helium implantation.

$B_{11}C$-CBC			**B_{12}-CCC**		
Novacancies and impurity atoms	***LDA* τ (ps)**	***GGA* τ (ps)**	**Novacancies and impurity atoms**	***LDA* τ (ps)**	***GGA* τ (ps)**
bulk	341	441	bulk	348	468
3H interstitials	286	334	3H interstitials	312	386
3He interstitials	258	355	3He interstitials	280	394
$1V_B$	354	464	$1V_B$	363	496
$1V_C$	354	464	$1V_C$	363	496
$1V_B$ in center of the chain	354	464	$1V_C$ in center of the chain	363	496
$1V_C$+$11V_B$	374	522	12 V_B	374	536
$1V_C$+$11V_B$ 1H nearly to C atom	373	516	12 V_B 1H nearly to C atom	373	580
$1V_C$+$11V_B$with 2H in center cluster	350	436	12 V_B with 2H in center cluster	359	461
$1V_C$+$11V_B$ 2H nearly to C	372.2	515	12 V_B 2H nearly to C	372.7	532
$1V_C$+$11V_B$with 4H in center cluster	349	428	12 V_B with 4H in center cluster	359	460
$1V_C$+$11V_B$with 2He in center cluster	326	469	12 V_B with 2 He in center cluster	339	498
$1V_C$+$11V_B$with 4He in center cluster	309	453	12 V_B with 4 He in center cluster	330	487

The picture shown in Figure 15 represents the largest volume of the defect which was be created in our super cell of B_4C, with the vacancy cluster being created by successively removing the nearest boron atoms to the defect position.

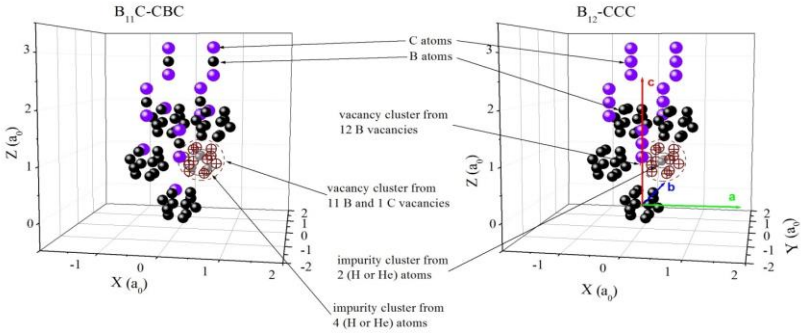

Figure 15. Visualization of super cell of B_4C and positions of point defects in vacancy cluster from 12 vacancies impurity with H or He atoms. **b**= $2a_0 sin(\alpha/2)$, α = 65.981°, There are presented two cases; fist polarized $B_{11}C$-CBC and second B_{12}-CCC.

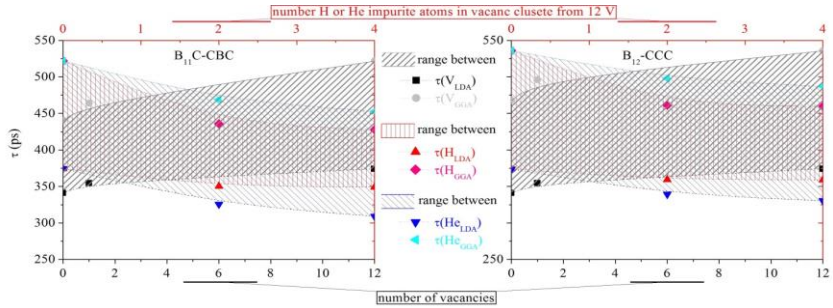

Figure 16. Functional dependencies between τ and number of vacancies or H and He atoms in vacancy cluster from 12 vacancies. There were made range between τ functions of LDA and GGA methods.

The cases of implanted H and He atoms in the internodes were also considered. The lower τ value of the $B_{11}C$-CBC combination compared to B_{12}-CCC confirms that the more physically optimized version of B_4C is $B_{11}C$-CBC. It is significant that the Doppler broadening of the spectrum is mainly considered in them, but the τ results are somehow neglected. In our work, we have tried to make up for this omission. The number of vacancies to the τ and the number of impurities to τ was plotted and presented in Figure 16. A slight deviation of the τ was observed regardless of the type of atoms

removed or added to the B_{12}-CCC. Accordingly, the difference between τ with the saturation of H or He defect is nearly 20 ps. If a comparison is made under the same conditions with $B_{11}C$-CBC, approximately twice the value for the same deviation will be seen. The range between LDA and GGA in B_{12}-CCCis wider then in $B_{11}C$-CBC. This should be interpreted as a better proximity to the physical optimization of the modification $B_{11}C$-CBC. Experimental results should be in the presented ranges between LDA and GGA results. Overall, a relatively small range of variation means that the type of defect in the B_4C material will give negligible change in the electron density. At the same time, we can conclude that in areas with a small temperature gradient, sintered materials with the B_4C component may be suitable for removing helium or hydrogen from the reactor walls (which are undesirable after synthesis). A substantial reason for this conclusion is due to the low electron density and large free volumes of the B_4C material.

In the presented **chapter**, the thermal flow function and heat capacity of boron nitride, boron silicate, boron carbide and boron oxide compounds at room temperature after irirradiation at 5.0×10^{12} ion/cm^2, 5.0×10^{13} ion/cm^2 and 3.83×10^{14} ion/cm^2 intensities with ^{137}Xe ions with 167 MeV energy were studied. Since the most effective study of the interaction of heavy ions with target samples and the temperature kinetics of the mechanism of defect formation in surface morphology has been studied at low temperature values, the main direction of research materials is focused on this temperature range. The spectra of DSC curves at different intensities for non-radiated boron nitride and boron oxide samples, which are a function of the heat flow, are given in Figure 17. The analysis of the thermal kinetics of the heat flow in the obtained spectra and the analysis of the thermal function in the given range of $120\leq T\leq300$K depending on the temperature were carried out. In both study samples, the heat flow value varies between -2 mW and a maximum of 2 mW. Given the initial and final values of the heat flow, the heating rate (heating rate of the sample in an argon medium), the mass and the calibration factors, it is possible to make certain analytical views on the mechanism of thermal kinetics. In boron nitride and boron oxide

samples, the DSC kinetics are not broken down into any parts as a thermal region after irirradiation with heavy ions of different intensities.

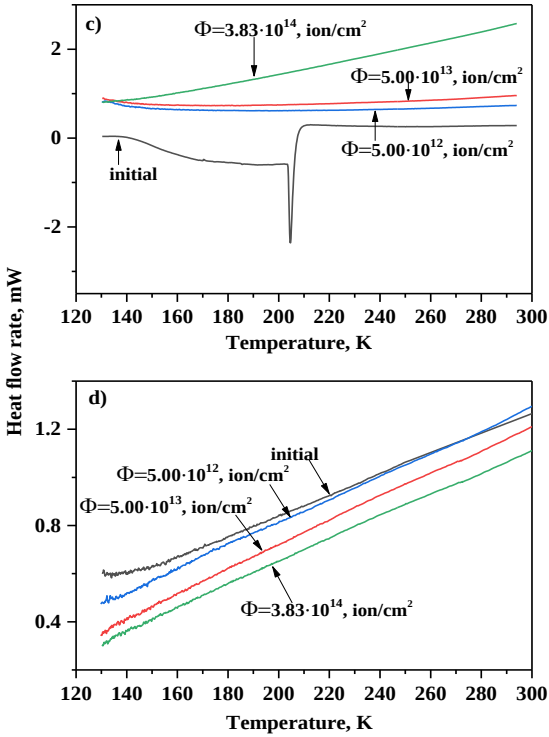

Figure 17. Boron nitride irradiated at 5.0×10^{12} ion/cm^2, 5.0×10^{13} ion/cm^2 və 3.83×10^{14} ion/cm^2 intensities in the temperature range $120\leq T\leq300$ K a) and boron oxide b) temperature dependence of the heat flow of the compounds.

However, in the unirradiated boron nitride sample, the value of the heat flow increases in the temperature range from 135K to 190K, which corresponds to the central peak of 217K, and the specific heat capacity of the sample increases monotonously in that temperature range. However, it is possible to show a change in a number of thermophysical parameters of the phase transition (specific heat capacity 3.02 J/g×K, activation energy 0.23 J×mol and enthalpy 0.0213 J/g), but not the specific heat capacity of the phase transition

with a central peak of 217K. A comparison of the thermophysical parameters of the effects with a central peak of 217K after irirradiation shows that the kinetics under the influence of heavy ions change with a more complex mechanism. In a non-irradiated boron nitride sample, the heat transfer and the flow change are completely different after both irirradiations.

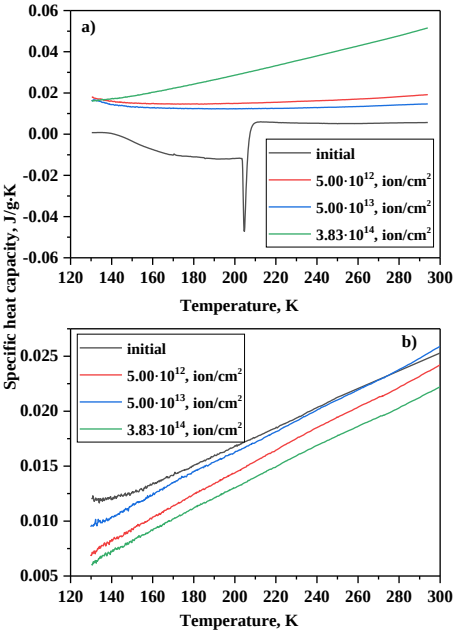

Figure 18. Boron nitride irradiated at 5.0×10^{12} ion/cm^2, 5.0×10^{13} ion/cm^2 və 3.83×10^{14} ion/cm^2 intensities in the temperature range $120\leq T\leq300$K a) and boron oxide b) temperature dependence of the specific heat capacity of the compounds.

In samples of boron nitride and boron oxide, the transfer of heat flow in the temperature range of $120\geq T\geq300$K varies in different phases. The thermal kinetics of varying phases is explained by the specific heat capacity. The kinetics of the spectra obtained for irradiated samples varies with linear regularity and the mechanism of all thermophysical processes that occur is explained by the heat capacity. The temperature dependence of the specific heat capacity of boron nitride and boron oxide compounds irradiated at 5.0×10^{12}

ion/cm^2, 5.0×10^{13} ion/cm^2 və 3.83×10^{14} ion/cm^2 intensities in the temperature range $120\leq T\leq300$K is given (Figure 18). In the unirradiated boron nitride sample, the value of the heat capacity is observed to increase in the temperature range $T\leq210$K. The value of the heat capacity of the unirradiated sample in the phase transition corresponding to the central peak 217K varies in the range 0.007-0.013 J/g×K. Also, before irirradiation with heavy ions, the value of the specific heat capacity increases to 0.0053 J/g×K and acquires a constant value in the temperature range from 200K to 300K. However, at 5.0×10^{12} ion/cm^2 and 5.0×10^{13} ion/cm^2 intensities, the change in the value of the heat capacity is small, and in the specified temperature range, the value of the specific heat capacity increases in the range of 0.0127 J/g×K and 0.0153 J/g×K. At a irradiation intensity of 3.83×10^{14} ion/cm^2, the value of the heat capacity varies from 0.0165 J/g×K to 0.0515 J/g×K. It is clear that the value of heat capacity is constant in samples irradiated at 5.0×10^{12} ion/cm^2 and 5.0×10^{13} ion/cm^2 intensities. It was found that the value of the specific heat capacity in the combination of heavy ions irradiated with heavy ions with 5.0×10^{12} ion/cm^2, 5.0×10^{13} ion/cm^2 and 3.83×10^{14} ion/cm^2 density of flows can be expressed as follows in the temperature range $120\leq T\leq300$K.

- ✓ Non-irradiated boron oxide sample; $0.0125\leq C_p\leq0.0262$ J/g×K
- ✓ 5.0×10^{12} ion/cm^2; $0.0099\leq C_p\leq0.025$ J/g×K
- ✓ 5.0×10^{13} ion/cm; $0.007\leq C_p\leq0.024$ J/g×K
- ✓ 3.83×10^{14} ion/cm^2; $0.006\leq C_p\leq0.022$ J/g×K

The kinetics of the change in heat capacity in the combination of boron nitride and boron oxide have been found to be similar to the heating mechanism of samples when irradiated with fast heavy ions. The results of experiments show that the heating of the boron nitride sample at low temperatures occurs by a dual mechanism. In our experimental studies, after irirradiation with heavy ions in a sample of boron carbide, the heat transfer mechanism in the temperature range of $120\geq T\geq146$K occurs in a small speed, $146\geq T\geq300$K in the more active phase. Also, for B_6Si compounds, heat transfer is the same as for boron carbide. According to the linear law, no phase change is observed in the changing kinetics, the heat flow value decreases to -

1.4 mW for B_6Si and 3.0 mW for B_4C. All thermophysical processes are based on a heat capacity at variable certain intervals and are interconnected. Figure 19 shows the temperature dependence of the specific heat capacity of 5.0×10^{12} ion/cm^2, 5.0×10^{13} ion/cm^2 and 3.83×10^{14} ion/cm^2 at different irradiations in the temperature range $120\leq T\leq300$K for samples of boron carbide and boron silicate.

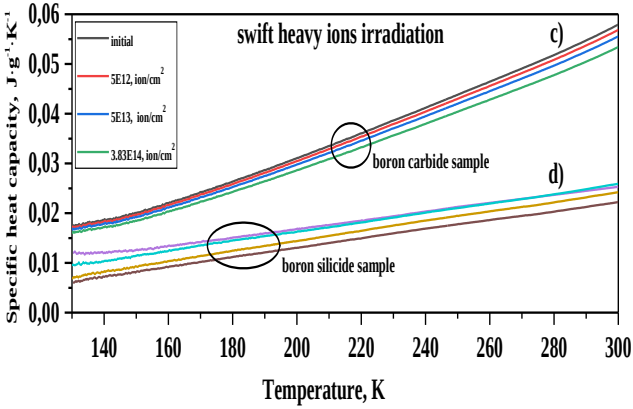

Figure 19. Boron carbide irradiated at 5.0×10^{12} ion/cm^2, 5.0×10^{13} ion/cm^2 and 3.83×10^{14} ion/cm^2 intensities in the temperature range $120\leq T\leq300$K c) and boron silicate d) temperature dependence of the specific heat capacity of the compounds.

The temperature-dependent kinetics of the heat flow reflects the temperature dependence of the heat capacity. From the temperature dependence of the heat capacity, it is clear that B_4C samples are equal to 0.0170-0.0176 J/g×K at 120K when exposed to ions of different intensities. However, the specific heat capacity of boron carbide samples irradiated with high-energy heavy ions varies from 0.016 J/g×K. The process is related to the kinetics of the mechanism of interaction with heavy ions, the amorphization of the surface morphology affects the kinetics of heat dissipation. It was also found that the B_6Si samples were non-irradiated and that the thermal conductivity mechanism differed slightly from that of the boron carbide sample, regardless of the irradiation intensity. In the B_6Si example, the heat distribution mechanism is a line. The kinetics of the specific heat capacity are given in Figure 20 for the B_4C and B_6Si

samples. The kinetics of changes in specific heat capacity show that boron carbide increases 3.59 times when exposed to fast heavy ions in the temperature range 120≤T≤300 K. For a boron silicon research sample, the specific heat capacity is increased 4.42 times by heavy ions. Experiments show that the value of specific heat capacity in boron silicon samples increases more rapidly. In addition, in all experimental experiments, changes in specific heat capacity in the more active phase after irirradiation with pain ions completely complement each other. The thermal conductivity values for the non-irradiated boron carbide sample increase in the temperature range 120K-300K from 0.0206 W/cm×K to 0.0674 W/cm×K. In the temperature range of 120-300K, it was found that the thermal conductivity of boron carbide samples increases in the range of 0.0193-0.0659 W/cm×K, 0.0188-0.0645 W/cm×K və 0.0181-0.0619 W/cm×K at an intensity of 5.0×10^{12} ion/cm^2, 5.0×10^{13} ion/cm^2 and 3.83×10^{14} ion/cm^2 during irirradiation with heavy ions Xe. However, the thermal conductivity values for the boron silicide sample under heavy ionizing irradiation increase from 0.014 to 0.026 W/cm×K in the temperature range of 120K to 300K for the non-irradiated sample. For samples of boron silicide irradiated at 5.0×10^{12} ion/cm^2, 5.0×10^{13} ion/cm^2 and 3.83×10^{14} ion/cm^2 intensity, the thermal conductivity in the temperature range of 120-300K was 0.0112-0.026 W/cm×K, 0.005-0.024 W/cm×K and 0.006-0.022 W/cm×K.

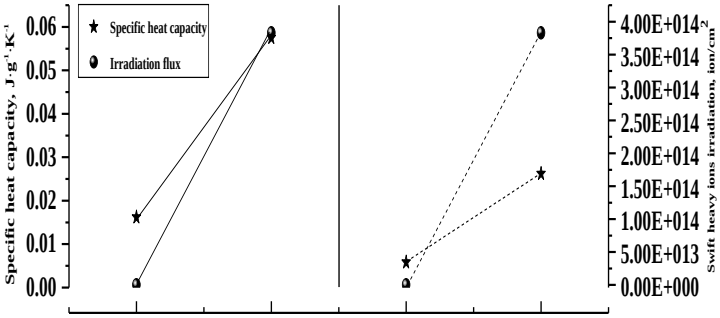

Figure 20. Kinetics of specific heat capacity of B_4C and B_6Si samples irradiated with heavy ions of different intensities in the temperature range 120≤T≤300K.

In boron carbide and boron silicide samples, the holes formed by irradiation oscillate between the C-C and Si-Si atoms. Due to the distribution mechanism of the pores, they move along the C-C and Si-Si chains, as well as the icosahedral chain at the boron-carbon junction. In single-phase boron-based compounds, the motion of the holes varies only between two carbon atoms and an inter-icosahedral chain. It is more obvious that the thermal conductivity for boron carbide compounds decreases from 0.1 to 0.01 W/cm×K for high temperature transition mechanism. However, in our experiments, the mechanism of conductivity at low temperatures is completely different. Due to the structural structure, the thermal conductivity at low temperatures depends on the dynamics of the lattice parameters. After irirradiation, the thermal conductivity of boron carbide and boron silicide samples increases. In this case, the radicals formed around the carbon and silicon atoms are involved in the heat transfer after irirradiation. After irirradiation, the thermal conductivity of the B_4C and B_6Si samples increases, and radicals formed around the carbon and silicon atoms after the heat carrier irirradiation are also present. However, this is not obvious because the recombination rate is lower at lower temperatures. Of course, the thermal conductivity is transmitted by a broken structure. It should also be noted that recombination rate at low temperatures is an important factor. It should also be noted that recombination rates at low temperatures are an important factor, and the low rate of thermal transfer in an amorphous structure depends on the repetitive chain behavior in the structure. However, for boron carbide irradiated with heavy ions at a temperature of 5.0×10^{12} ion/cm^2, 5.0×10^{13} ion/cm^2 and 3.83×10^{14} ion/cm^2 at a low temperature of T≥179K, the thermodiffusion value decreases to 0.475 cm^2/sec, 0.462 cm^2/sec and 0.397 cm^2/sec, respectively. The thermodiffusion value of boron silicide samples with different heavy ions at different intensities was 0.35-0.47 cm^2/sec, 0.36-0.46 cm^2/sec and 0.38-0.49 cm^2/sec.

In the sixth chapter of the dissertation the compounds B_2O_3, B_4C, B_6Si and BN were irradiated with absorption doses of 9.7 kGr, 48.5 kGy, 97 kGy, 145.5 kGy and 194 kGy with ^{60}Co isotope with dose strength D=0.27 Gy/sec with power line 1.25 MeV and

thermophysical properties were studied by differential scanning calorimetric method. Thermodynamic functions depending on small and high absorption doses of gamma irradiation, explanation of the increase of energy levels in the crystal structure with color centers, transition to amorphous phase, active centers formed in the sample, thickness of oxide layers on the crystal and kinetic substantiation of formed defects. The temperature-dependent variation of Janderson curves in B_4C and B_6Si crystalline structures depending on gamma absorption doses has been extensively analyzed. Figure 21-24 shows the surface morphology of samples irradiated at different doses with a purity of 99.5% boron carbide, 99.8% boron silicate, 99.2% boron nitride and boron oxide. Samples studied under special laboratory conditions are added to thin layers of carbon with a uniform distribution of 1-3 mm thickness and placed in an experimental chamber at a high vacuum level. With the help of the SE2 detector, the energy of the electron stream is increased in small steps according to the surface relief, detailed information on the distribution of particles and the distribution of measurement are obtained. Depending on the irradiation dose, traces of amorphization are found, marked with red circles of 97 kGy, 145.5 kGy and 194 kGy. No traces of amorphization are found in small doses. For boron carbide compounds, it has been determined that the size of microcrystals varies in the range of 5-7 μm. The specific hardness of the boron carbide sample, the aggregation of water molecules absorbed from the atmosphere by the active surface is not observed at a given size, and the particles are located completely differently from each other.

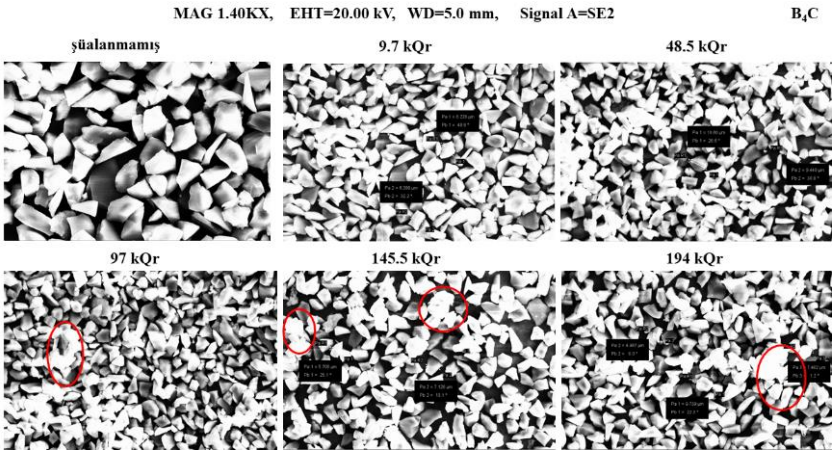

Figure 21. Irradiated surface morphology of B_4C at absorption doses of 9.7 kGy, 48.5 kGy, 97 kGy, 145.5 kGy and 194 kGy.

Figure 22 shows the surface morphology of the B_6Si compound obtained with 20.00 keV electrons with the SE2 detector.

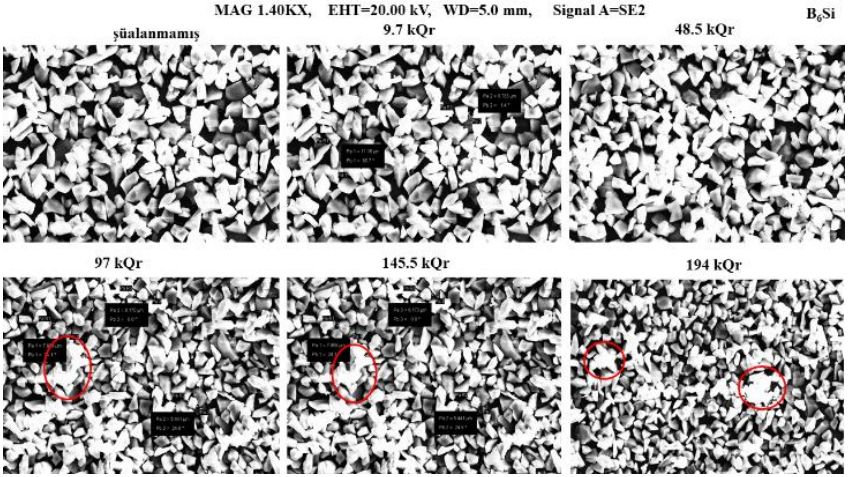

Figure 22. Irradiated surface morphology of B_6Si at absorption doses of 9.7 kGy, 48.5 kGy, 97 kGy, 145.5 kGy and 194 kGy.

Due to the morphological properties of the surface, the distribution of particles in the silicon boride compound varies. It is

clear from the figure that boron and its various compounds do not have a spiral shape. Spiral formation is more common in orthorhombic compounds. In contrast to boron carbide, traces of amorphization are observed in boron silicate compounds starting from a gamma absorption dose of 48.5 kGy. The mechanism of amorphization under the influence of gamma rays occurs in a weaker phase than boron carbide compounds. Measurements made at the selected area in the magnified area show that in the B_6Si sample, the particles were not the same size and were distributed along the surface in different sizes. The average size of boron silicate microcrystals varies in the range of 5-80 μm.

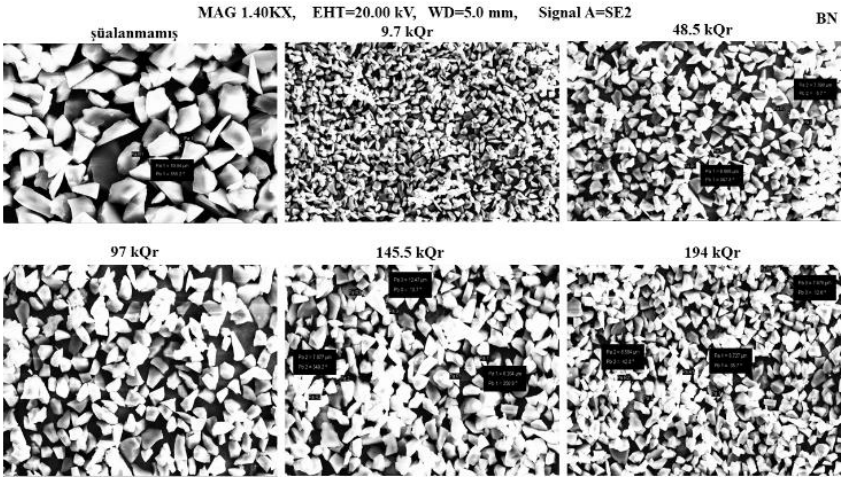

Figure 23. Irradiated surface morphology of BN compound at absorption doses of 9.7 kGy, 48.5 kGy, 97 kGy, 145.5 kGy and 194 kGy.

On the other hand, the surface morphology of boron nitride compounds is identical to that of boron carbide and boron silicate samples. The measurements made at the selected points show that in the boron-nitride sample, none of the particles were the same size and were distributed along the surface in different sizes. In boron-nitride samples, the measurement is in the range of 52÷120 μm. The formation of the amorphous phase is not observed. Figure 24 shows the surface morphology of a nano-sized B_2O_3 compound depending on the gamma irradiation dose. In the studied range of 500 nm, no

significant change in the surface of the crystals occurs in the dose range of 9.7 kGy to 48.5 kGy. Starting from the absorption dose of 97 kGy, the mechanism of surface degradation at the maximum absorption dose of 194 kGy creates a mechanism for the formation of a layered broken structure at the atomic level. Experiments have shown that particles ranging in size from 32 μm to a maximum of 120 μm are found in the samples. SEM studies have shown that particle size distribution varies in the combination of boron silicate, boron carbide, boron nitride, and boron oxide.

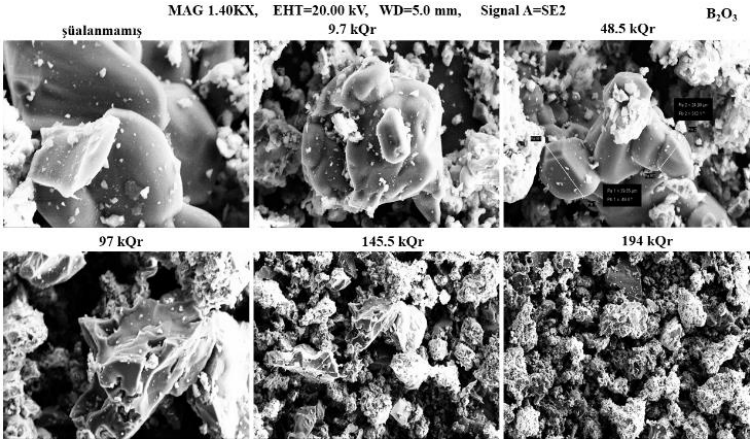

Figure 24. Irradiated surface morphology of B_2O_3 in absorption doses of 9.7 kGy, 48.5 kGy, 97 kGy, 145.5 kGy and 194 kGy.

It was also found that the analysis of the composition of the compounds revealed the presence of small amounts of mixed elements. SEM studies have shown that after irirradiation of the samples with 145.5 kGy of gamma rays, traces of amorphization are found on the surface, and amorphization is clearly distinguished after absorption doses of 194 kGy. Element mapping analysis was performed in the selected section of 100 μm for boron carbide bonding. In non-irradiated and irradiated samples at different times, the dynamics of changes of particles and chemical elements on the surface are given. Although the distribution of particles and elements in the mapping of elements in non-irradiated samples is close to a homogeneous form, the mapping of elements in irradiated samples in

a selected time interval is different. At first glance, it is clear that the distribution of particles on the surface is more heterogeneous. More combination of C, Si, Ca and O elements with increasing irradiation time of the main mechanism in the mapping of elements after irirradiation, ie the mobile accumulation in one part or in different parts. In addition to the results obtained from SEM studies, structural analyzes were performed on B_4C and B_6Si samples. X-ray diffraction spectra of the crystal structure of the B_4C compound before irirradiation and after irirradiation at different absorption doses are given in Figure 25.a. The crystal structure of the B_4C compound from the diffraction spectra has a rhombohedric symmetry of the *R*-3m space group, which is consistent with previous research results. Diffraction spectra obtained during irirradiation at an absorption dose of 194 kGy show that the background of the spectra changes as the irradiation dose increases. This corresponds to the collapse of the crystal structure and amorphization under the influence of irradiation. Figure 25.b shows a comparison of the backgrounds of the spectra obtained without irradiation and at the highest irradiation dose. In the X-ray diffraction spectra, maxima were observed in the range of 25–30 ° that did not relate to the structural structure of the B_4C compound (Figure 25.c). The analysis revealed that these maxima correspond to graphite and O-H groups. Diffraction peaks corresponding to graphite are not observed after 97 kGy of irradiation, and diffraction peaks corresponding to hydroxide groups are not observed after 194 kGy of irradiation. Under normal atmospheric conditions and room temperature, the values of the lattice parameters of the B_4C compound were determined a = 5.630 (2) Å and c = 12.151 (4) Å. As can be seen from the graph, there was no structural phase transition in the structure up to the absorption dose of 194 kGy, only an increase in the values of the lattice parameters was observed, which is explained by the rupture of interatomic bonds under the influence of gamma rays. The dependence of the lattice parameters on the irradiation absorption dose is given in Figure 26.a. The curves show that although the values of the lattice parameters increase more rapidly at small doses of irradiation, the rate of increase of the lattice parameters values after irirradiation at an absorption dose of 145.5 kGy stabilizes.

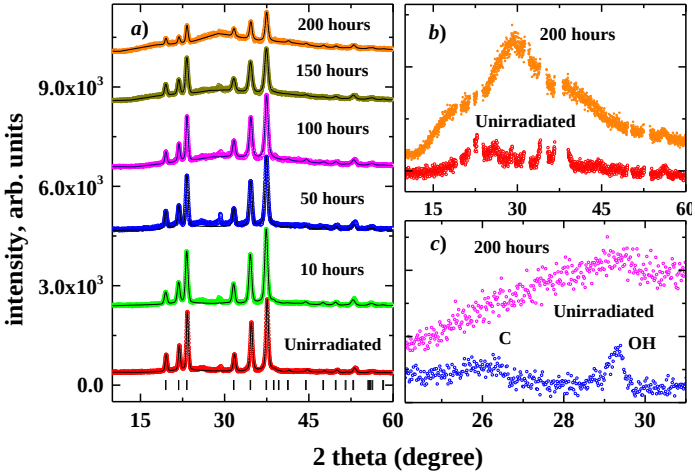

Figure 25. a) X-ray diffraction spectra of a B_4C compound irradiated at different absorption doses at room temperature and under normal atmospheric conditions, b) X-ray diffraction spectra of non-irradiated and 194 kGy irradiated B_4C compound, c) X-ray diffraction of graphite and hydroxide group.

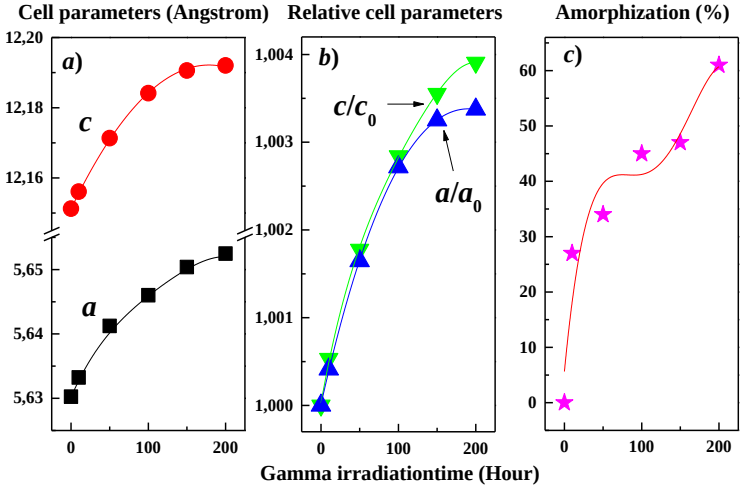

Figure 26. a) The dependence of the lattice parameters of the B_4C compound, b) the relative lattice parameters of the B_4C compound, c) the irradiation dose dependence of the amorphous mechanism in B_4C crystals.

It can be assumed that irradiation at absorbed doses of more than 97 kGy causes destabilization in the crystal lattice, the breakdown of inter-atomic bonds and structural changes. After irirradiation at absorption doses of 145.5 kGy, these processes stabilize. It is obtained from the irradiation dependence of the values of the lattice parameters that the value of parameter c (0.39%) increases more than the value of parameter a (0.33%). This is due to the fact that long bonds are weaker and more prone to breakage as a result of external influences. Due to their higher energy with short bonds, they are also resistant to external influences. In order to more clearly show the mechanism of change of lattice parameters depending on the irradiation dose, Figure 26.b shows the dependence of the relative values of the lattice parameters a/a_0 and c/c_0 on the irradiation dose. It has been found that increasing the irradiation dose causes the peaks to expand and the background to form. In X-ray diffraction spectra by the method of fully integrated background area, the dependence of the percentage of amorphization on the irradiation dose was determined (Figure 26.c). It is clear from the results that after irirradiation at absorption doses of 194 kGy, complete amorphization did not occur in B_4C crystals, 38% of the crystal structure was preserved.

The B_6Si sample was irradiated with gamma quanta at room temperature at different absorption doses, and the structural spectra obtained for the samples before and after irirradiation were shown in Figure 24. From the spectra obtained for the non-irradiated B_6Si sample, it is clear that the compound has a crystalline structure. The values of the lattice parameters for the non-irradiated sample are in the form a = 14.0605 (5) Å, b = 18.0279 (2) Å and c = 9.2692 (7) Å. The results showed that at normal atmospheric pressure and room temperature, the B_6Si sample has the *Pnnm* space group and symmetry of the orthorhombic crystal structure. The experimental results obtained for the non-irradiated boron silicate sample are similar to those of other studies. Intensity changes in diffraction peaks were observed for gamma-irradiated samples in the absorption dose range of $0 \leq D \leq 97$ kGy. Spectral fluctuations were observed at the absorption dose of $0 \leq D \leq 97$ kGy in the intensity of B_6Si-specific peaks.

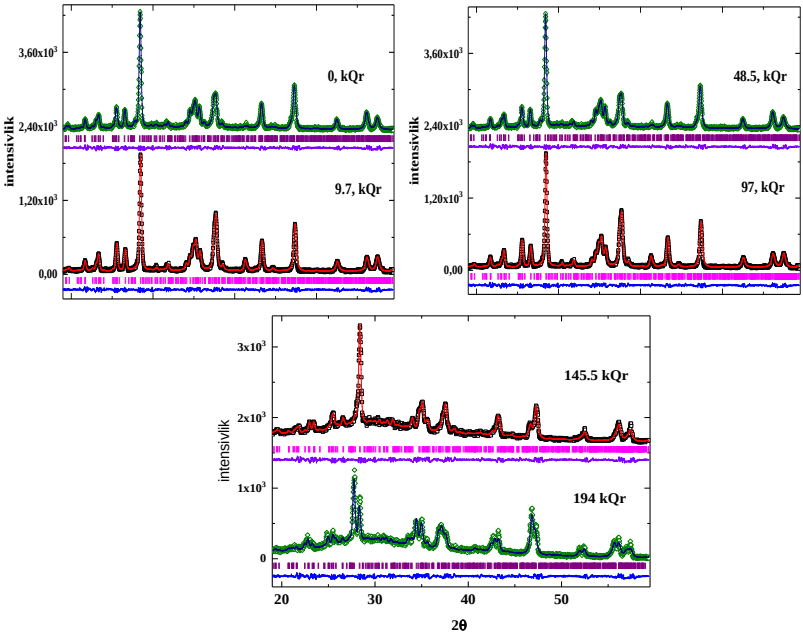

Figure 27. Structural spectra for B_6Si sample at absorption doses of 9.7 kGy, 48.5 kGy, 97 kGy, 145.5 kGy and 194 kGy for gamma irradiation.

The change in the intensity of the peaks can be explained by the crystal structural changes of the samples. At given irradiation, the crystal structure *Pnnm* maintains the symmetry of the space group. This decrease occurs under the influence of 1.2 MeV gamma quanta and the values of the lattice parameters change (this applies to the ideal state of some atoms). Starting from the absorption dose D≥145.5 kGy, the partial amorphization mechanism begins in the B_6Si sample. To determine the degree of amorphization in the sample, the area formed by the peaks of the non-irradiated sample is divided into the areas of the peaks of the irradiated samples. Also, when the gamma adsorption dose is increased after D≥145.5 kGy, some diffraction intensity of the spectra decreases. Figure 25 shows the amorphization rate in a B_6Si sample depending on the gamma irradiation dose. At the absorption dose of 145.5 kGy, the amorphization rate was 54%, and at the adsorption dose of 194 kGy was 69%.

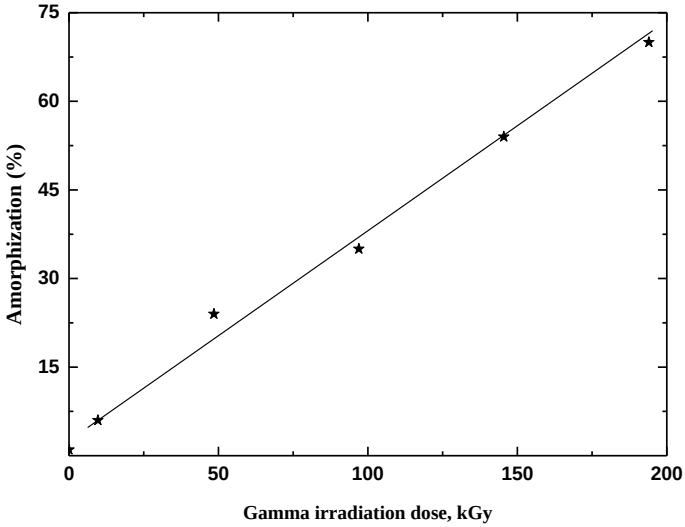

Figure 28. Degree of amorphization depending on the dose of gamma irradiation.

The lattice parameters of the B_6Si sample were calculated by the Ritveld method, depending on the absorption doses of gamma irradiation, the value of the lattice parameters increases to a = 0.164 Å, b = 0.009 Å, c = 0.09 Å and the volume of the crystal structure reaches V=30,9 $Å^3$. The changes in the observed parameters and volume of the elemental lattice in the irradiated B_6Si combination are given in Table 4. The results in table 4 show that the lattice parameters increase with the irradiation dose, the lattice parameter for the non-irradiated sample varies between 14,060 Å, 48.5 kGy and 194 kGy, and the lattice parameters vary between 14,096 Å and 15,224 Å, respectively. With increasing irradiation dose, the volume of samples increased from 2349 $Å^3$ before irirradiation to 48.5 kGr after irirradiation to 2356 $Å^3$ and 2380 $Å^3$, respectively. The increase in the volume and parameters of the lattice indicates the influence of external factors on the material. The B_6Si sample is shown in Figure 26 of the mechanism for changing the lattice parameters a, b, and c depending on the gamma absorption dose. Irradiation coefficients were calculated using the following equation.

$$K_i = \left(\frac{1}{a_{io}}\right)\left(\frac{da_i}{dD}\right)_{P,T}$$

Where $K_i$is the coefficient of expansion, a_{io} is the lattice parameters of the unirradiated sample, a_i is the lattice parameters of the irradiated sample, and D is the absorbed dose due to gamma irradiation.

Table 4. Lattice parameters and volume in B_6Si combination irradiated at different absorption doses.

Gamma dose, (kQr)	Lattice parameters and volume			
	a, Å	*b*, Å	*c*, Å	*V*, Å^3
0	14.060(6)	18.027(9)	9.269(2)	2349.(6)
9.7	14.072(2)	18.028(6)	9.269(7)	2351.(8)
48.5	14.096(5)	18.030(3)	9.271(3)	2356.(4)
97	14.156(9)	18.032(2)	9.274(2)	2367.(5)
145.5	14.190(2)	18.034(2)	9.276(5)	2373.(9)
194	14.224(7)	18.036(2)	9.278(4)	2380.(5)

As a result, the values obtained for K_i (linear expansion of the lattice parameters) were determined as $k_a = 6.2\times10^{-5}$ kGy^{-1}, $k_b = 2.3\times10^{-6}$ kGy^{-1}, and $k_c = 5.2\times10^{-6}$ kGy^{-1}. As can be seen from the last graph, an increase in the absorption dose of gamma irradiation results in an increase in the volume of the B_6Si lattice. In addition, the increase in lattice volume from V_0 = 2349. (6) Å^3 to $V_{194\ kGy}$ = 2380. (5) Å^3 indicates a 1.31% increase in lattice volume. It became clear that no phase transition occurred as a result of gamma irradiation in the lattice structure. The intensity and energy of gamma irradiation change the coordinates of the atoms in the lattice, and the law of distant order is violated. At high absorption doses, gamma irradiation forms various point defects and active centers that can migrate in the sample, which is described in detail in the next section. B_4C samples irradiated with gamma rays (diameter 7 mkm, thickness 200-500 nm and scanning speed 600 nm / min) were measured using UV-V Gary 50 Scan spectrophotometer. Optical absorption spectra were collected in the wavelength range of 200-800 nm. 460 nm of absorption bands of F-type color centers and 700 nm of M color centers are observed. F^+ color centers with activation energies of 1.89 eV at wavelengths of 212

nm, 300 nm, 374 nm and 434 nm were observed from the main spectrum of the B_4C sample. Two M color centers were detected at 561 nm and 648 nm with activation energy 0.1 eV in the same absorption spectrum. After irirradiation of 48.5 kGy of gamma, the intensity of the peaks, which characterizes the absorption of F^+ color centers, increases.

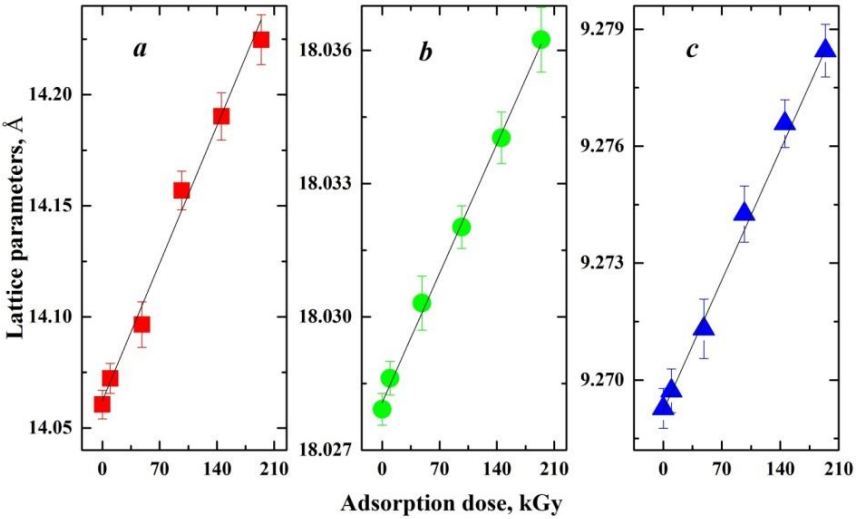

Figure 29. Adsorption dose dependence of B_6Si lattice parameters. Lines are the interpolation of experimental data with polynomials of linear functions.

With increasing dose of gamma irradiation, the absorption spectra of F^+ color centers increase from 145.5 to 194 kGy. This increase was faster at high irradiation doses. In this experiment, at low gamma irradiation doses, there was no change in the color center from F to F^+, because the irradiation was carried out at room temperature for all samples. The chapter also examines the mechanism of oxidation of ceramic materials at high temperatures in experimental studies. Oxidation in the B_6Si compound begins at $T \geq 650°C$, respectively, for non-irradiated and irradiated samples at absorption doses of 9.7 kGr, 48.5 kGy, 97 kGy, 145.5 kGy, and 194 kGy. However, depending on the irradiation absorption dose in the region of $T \leq 650°C$, different amounts of decomposition are observed in the mass of the samples,

which is due to the decomposition of water vapor assimilated by the samples under atmospheric conditions. The degree of oxidation depends on the dose absorbed, mainly in two parts; The non-isothermal region starts in the temperature range of 650≤T≤740°C and the isothermal T≥740°C. The critical oxidation temperature for the sample is 970°C at absorption doses of 9.7 kGy, 48.5 kGy, 97 kGy, 145.5 kGy and 194 kGy. A small percentage of oxidation in the non-isothermal region indicates that the oxidation mechanism is passive. The formation of a liquid B_2O_3 layer on the surface of B_6Si particles is more active in the isothermal region. Oxidation in a non-irradiated sample is 3.5%, while in an irradiated sample of 194 kGy it is 8.2%. Experimental results show that a two-mechanism oxidation process takes place. After the critical temperature, the oxidation process in the active phase of B_6Si particles is completed. To determine the kinetics of the oxidation process and the activation energy, the time dependence of the process must be determined at different absorption doses. The dependence of the oxidation rate with increasing temperature at different absorption doses over time for the B6Si compound is shown in Figure 30. At T≤650 y°C, the oxidation states at all absorption doses are approximately equal. Also, no oxidation is observed at low values at the melting temperature of B_2O_3 (T= 450 °C). This is because the temperature range 450≤T≤650 °C is a thermally stable region in the sample, and the heat flow rate does not cause any dynamic change in the sample. Oxidation of the B6Si compound after irirradiation at a low temperature of ≤650°C is more of a "non-isothermal oxidation". However, after 70 minutes at T≥740°C, linear oxidation is observed throughout the region, regardless of the absorption dose, and this value increases until it reaches a critical limit. Dependence of the degree of oxidation on temperature, irradiation absorption dose and time showed that the main oxide layer is surface. Determines the depth of oxidation and the rate of diffusion of oxidation and the level of the critical limit in surface oxidation processes. The depth of oxidation at the surface depends on the molar mass of the sample, the molar mass of the compounds formed after chemical conversion, the specific surface area of the particle and the size of the particle, as well as the absorption

dose and temperature of irradiation. Given the chemical transitions from B_6Si to B_2O_3 and SiO_2 in the oxidation reaction, the depth of the oxide formed at the surface and the depth of the oxide formed for each absorption dose can be calculated.

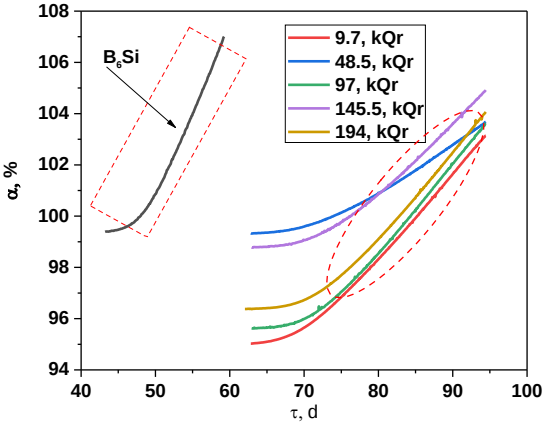

Figure 30. Time dependence of oxidation rate of B_6Si sample at different gamma irradiation doses in the temperature range $650 \leq T \leq 1000$ ° C

Figure 31 shows the dependence of the oxidation rate and the oxidation depth on the irradiation absorption dose. As expected, the degree of oxidation and the depth of oxidation occur by a dual mechanism $\alpha_\gamma + \alpha_T$, depending on the irradiation absorption dose and temperature. After an absorption dose of 97 kGy, a stable region begins both in the degree of oxidation and in the oxide layer formed on the surface. This dependence suggests that B_6Si is the critical limit for the 97 kGy oxide layer and the oxidation state for the compound. However, in different non-irradiated materials, the "critical limit" factor remains at different values and depths. Also, the fact that the specific surface area is a significant factor in the degree of oxidation and the high degree of chemical purity of the substance has a significant impact on the oxidation factor. As linearity and a stable region are observed in the oxidation process, the kinetics of this process are explained by the mechanism of the chemical reaction that takes place on the surface. In many cases, the mechanism of the surface oxidation layer occurs with different regularities.

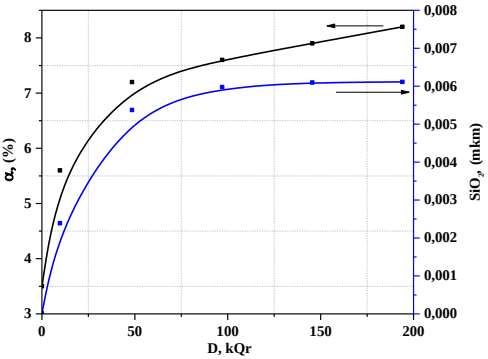

Figure 31. Oxidation rate in the temperature range 650≤T≤1000 ° C and the relationship between gamma irradiation dose and oxidation depth.

In explaining the kinetics of physical and chemical processes, the kinetics of the process is constructed using the k-diffusion rate coefficient. Oxidation kinetics in the temperature range 650≤T≤1000°C for B_6Si compounds were constructed using Jander's equation.

$$\left[1-(1-\alpha)^{\frac{1}{3}}\right]^2 = kt$$

Here α-oxidation rate, k-diffusion rate coefficient and t-reaction time. Figure 32 Jander curves were constructed depending on time and temperature for the B_6Si compound irradiated at different absorption doses. As can be seen, the Jander curves are divided into two parts in the temperature range 650≤T≤1000°C for the B_6Si compound irradiated at different absorption doses. Depending on the time, the temperature of 740°C characterizes the weak diffusion in the nonlinear part, ie passive oxidation, and the linear part characterizes the oxidation diffusion in the active phase. Oxidation diffusion at higher absorption doses and temperatures has been found to be more value effective. In addition, B_2O_3 and BO_2 evaporation reactions occur in parallel with the increase in mass in the oxidation reaction. However, since the rate of the evaporation reaction is lower than the rate of the oxidation reaction, the curves have a greater numerical value at high absorption doses of gamma irradiation. Since the SiO_2 evaporation reaction is 2230°C, SiO_2 only increases the diffusion rate

of oxidation. To be more precise, the oxidation reaction of $B_2O_3 + SiO_2$ occurs much faster than the evaporation reaction of B_2O_3 and BO_2. Figure 30 shows the Arrhenius curves for the oxide layer formed in the B_6Si compound irradiated at different absorption doses.

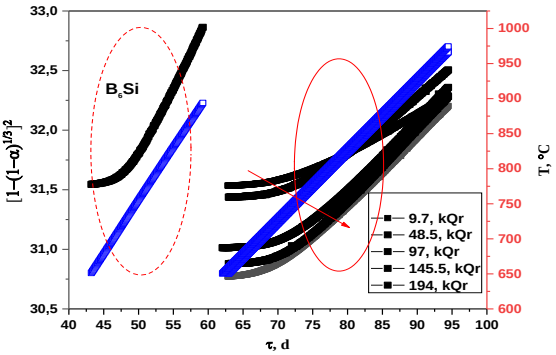

Figure 32. Jander curves at different gamma irradiation doses in the temperature range 650≤T≤1000°C

For this purpose, the dependence of the *lnk* logarithmic value of the diffusion rate of oxidation on the temperature opposite value of 1000/T was established. It was determined that for a non-irradiated sample, 21.3 kC/mol and 9.7 kGy, 48.5 kGy, 97 kGy, 145.5 kGy və 194 kGy receives a value of 41.5 kC/mol, 43.2 kC/mol, 45.3 kC/mol, 47.6 kC/mol, and 49.8 kC/mol, respectively, for absorption doses. The values obtained are close to the results of the standard values obtained for the non-radiated B_6Si. Changes in the value of activation energy show that the B_6Si compound irradiated at different times oxidizes at high temperatures and loses some degree of purity. The dependence of the activation energy on the absorbed dose of irradiation in Figure 0 once again confirms the above experimental results. After irirradiation of the B_4C compound with different gamma irradiation doses, samples were obtained at room temperature in the TG curves characterizing the mass kinetics by heating to 1230K (heating rate 5 K/min and measurement weight 13.5 mg). The mass curves of the irradiated B_4C samples are divided into three regions, respectively.

- 300≤T≤900K decreasing area
- 900≤T≤950K fixed area
- 950≤T≤1250K increasing area (oxidation reaction)

After gamma irradiation in B_4C samples, the rate of interaction with water vapor increases and the absorption properties of the compounds increase. However, interactions with water vapor and solvothermal chemical reactions in the temperature ranges of $300 \leq T \leq 900K$ are reported. In addition, the solvothermal chemical reaction of physical and chemical processes under the influence of gamma rays is complicated.

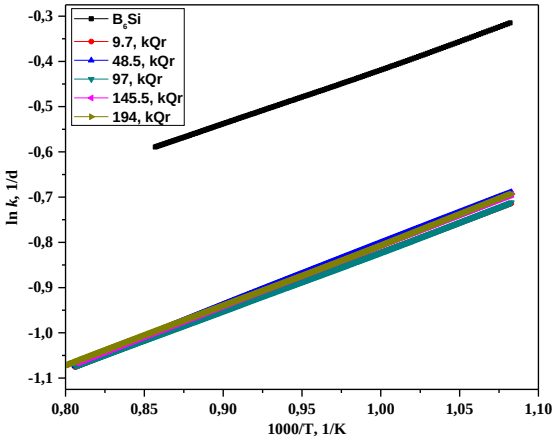

Figure 33. Arrenius curves at different gamma irradiation doses in the temperature range $650 \leq T \leq 1000°C$

On the other hand, adsorbed water molecules break down based on a complex gamma irradiation mechanism. The resulting hydrogen atoms and (OH) hydroxide groups are captured by structural defects, excited B atoms, free carbon, excited carbon atoms, and active sites. It also causes molecular hydrogenation. For hydrogen atoms, it can be schematically described as follows.

$$\gamma \xrightarrow{gamma\ irradiation} HOH \rightarrow H^+ + OH^-$$
$$H^+ + BC^* \rightarrow BC - H$$
$$H^* + C^* \rightarrow CH$$
$$H^* + H^* \rightarrow H_2$$
$$OH^* + OH^* \rightarrow HOH + O$$
$$OH^* + BC^* \rightarrow BC(OH)$$
$$OH^* + B^* \rightarrow B(OH)$$
$$O^* + B^* \rightarrow BO$$
$$O^* + C^* \rightarrow CO$$

The above schematic transitions can be found in some experimental experiments. Atmospheric conditions B_4C samples in powder form have various chemical reactions with water vapor. The dependence of the activation energy on the absorbed dose of irradiation in Figure 31 once again confirms the above-mentioned experimental results. The relationship between the oxidation state and the activation energy for each experiment performed at different absorption doses can be written as follows.

$$\left[\ln\left(\frac{dD_{\gamma i}}{dT_{\alpha}}\right)\right]_i = -A\cdot\left[\frac{E_T + E_{\gamma} + E_{Amorf}}{RT}\right] \qquad (6.4.6)$$

Here, D_i- is the absorption dose of ^{60}Co gamma source (30 rad / sec), T_{α}- is the oxidation temperature, E_T- is the temperature activation energy, E_{γ}- is the activation energy of the gamma source, and E_{Amorf}- is the activation energy of the amorphous amorphization.

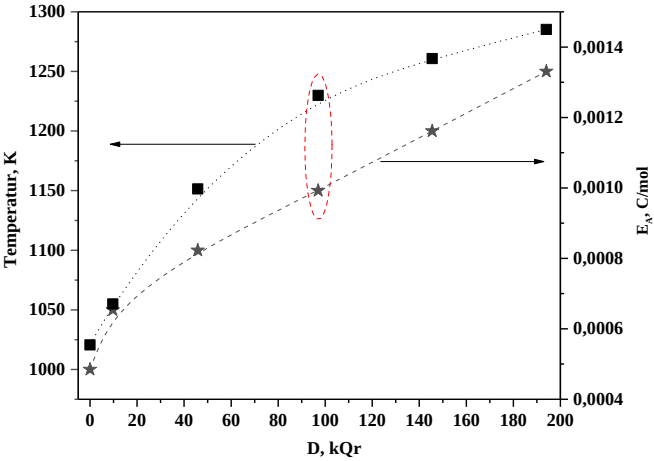

Figure 34. Activation energy of boron carbide samples at different gamma absorption doses

As shown in Figure 34, the change in kinetics of the activation energy depending on the temperature depends on the absorption dose of irradiation, which shows that the value of the activation energy increases with increasing irradiation absorption dose. At high absorption doses, as seen in all the parameters listed above, the values in Figure 34 are close to each other. As can be seen

from the depth value determined for the oxide layer, it is the complete capture of the oxygen atoms by the active sites at high absorption doses and the completion of the resulting oxidation reaction. The values of the activation energy determined for the oxide layer formed in the oxidation reaction by a complex mechanism are close to the maximum values obtained after the absorption dose. The mechanism of oxidation kinetics of boron carbide compounds with a high degree of purity under the influence of temperature and gamma irradiation has been studied in detail. TG analysis showed that studies of powdered boron carbide samples showed that the mass kinetics varied by different mechanisms depending on the temperature range. The decomposition of the hydroxide group in the boron carbide compound under the influence of gamma irradiation is also reflected. Depending on the irradiation absorption dose, the oxidation rate of boron carbide compounds with a high degree of purity is stabilized at high absorption doses. At high temperatures, the thickness of the oxide layer formed by non-isothermal oxidation increases depending on the irradiation absorption dose. Also, the change in diffusion rate in time-dependent kinetics and the value of the activation energy of the oxide layer formed after each absorption dose were determined.

In the last chapter, a comparative analysis of the experimental experiments performed on the chapters was performed. Depending on the type, intensity and energy of irradiation, attention is paid to the kinetics of important processes such as the mechanisms of displacement of atoms in the crystal structure, defect formation and recombination. Mutual comparison and substantiation of thermophysical parameters in research samples under the influence of heavy ions was performed. Molecular dynamics analyzes were carried out for research samples using high-capacity equipments, and the mechanism of surface effects degradation was explained.

MAIN RESULTS

1. The basics of the mechanism of decomposition of water molecules captured by the active surface of 80 nm B_2O_3 crystals with fast neutrons with 1 MeV energy in impulse mode depending on the intensity of the fast neutron flow are given. The effect of a fast neutron flow increases the intensity of the decomposition modes and leads to the formation of new functional groups 2900 cm^{-1}, 2989 cm^{-1}, 3676 cm^{-1}, 3735 cm^{-1}. Starting from the intensity of 1.3×10^{13} n/cm², the effects of OH groups, hydrate and hydroxide group on free and combined phases were observed. 1.3×10^{13} n/cm²-1.0×10^{15} n/cm² range of the neutron flow indicates that the hydroxide groups remain anionic and cationic in the crystal structure. Also, the internal force constants of the groups formed under the influence of neutron flow in the B_2O_3 nano crystal were determined to be 24.2-126.0 N/kg for B-O, 67.2-376.1 N/kg for B-OH and 75.4-125.8 N/kg for free OH.

2. Raman peaks at frequencies of 207 cm^{-1}, 498 cm^{-1}, 527 cm^{-1}, 883 cm^{-1}, 921 cm^{-1} and 1165 cm^{-1} were observed in nano B_2O_3 crystals under the influence of neutron flowes of different intensities. The displacement of the peaks at the Raman frequencies 883 cm^{-1}, 921 cm^{-1} and 1165 cm^{-1} indicates that the process of degradation (amorphization) has taken place on the surface of the samples. As the intensity of neutron flowes of different intensities with a energy of 1 MeV increases, the crystallinity of nano boron oxide increases from 90 nm to 138 nm.

3. Field energies were calculated in the temperature range $422\leq T\leq438$K and $438\leq T\leq443$K in the spectra characterizing the heat flow function in the temperature range $100\leq T\leq800$K of the nano B_2O_3 sample irradiated at the intensity 4.0×10^{12} n/cm², 8.0×10^{12} n/cm², 1.3×10^{13}, 4.0×10^{14} n/cm² and 1.0×10^{15} c/sm² . Double endo effects up to a temperature of 443K, a complex state of thermal velocity after 456K and thermal transitions occurring at high temperatures by the mechanism $B_2O_3\leftrightarrow HBO_2\leftrightarrow B(OH)_3$ and thermophysical parameters depending on the neutron flow were determined.

4. Wigner's energy kinetics (95.8 J/g for Wigner energy at 598K, 93.89 J/g at 623K and 94.49 J/g at 1002K) in the temperature range $300\leq T\leq1300$K was determined in boron nitride microcrystals

irradiated with neutron flow at different intensities. In a boron nitride sample of 1.0×10^{15} n/cm² intensity, the heat flow value was stable at 0.66 mW up to 467K, and in the following stages the heat flow value increased rapidly to 11.25 mW and the maximum value for the energy of the effect formed at the central peak 969 K was 373.609 J/g was found.

5. Regardless of the intensity of the electron flow, the kinetics of the change in specific heat capacity in the compounds is weak at low temperatures and increases rapidly at high temperatures. Mathematical equations expressing the temperature dependence of the specific heat capacity were obtained for all samples, in the B_4C sample, the value of thermal conductivity at 120K was 0.0243 W/cm×K, 0.02420 W/cm×K and 0.02401 W/cm×K, the value of thermal conductivity after irradiation at intensities 0.0247 W/cm×K, 4.16×10^{16}, 1.20×10^{17}, 1.03×10^{18} 1/cm^2, for the boron silicate sample, the value of thermal conductivity in the temperature range of 120-300 K was determined to vary from 0.0175-0.035 W/cm×K, 1.03×10^{18} 1/cm^2 to 0.009-0.0335 W/cm×K. The value of thermal diffusion was 0.791-0.806 cm^2/sec in the temperature range 100-300K for a boron carbide sample, 0.808-0.794 cm^2/sec for different intensities, 0.798-0.716 cm^2/sec, 0.767-0.690 cm^2/sec and the value of thermal diffusion for the boron silicate sample was 0.576-0.591 cm^2/sec, 0.577-0.579 cm^2/sec, 0.54-0.559 cm^2/sec, 0.44-0.566 cm^2/sec were determined at different intensities.

6. After irirradiation of B_2O_3, B_4C, B_6Si and BN compounds with fast heavy ^{132}Xe ions with an energy of 167 MeV, the dynamics of the distribution of nano-pin holes 18-20 nm was observed in the images of surface morphology, varying in the microstructure of swellings by area and size. Studies show that the growth rate of swellings on the surface of the samples is 2.2 times greater than in irradiated samples, and the growth rate of swellings on the surface of the samples is 0.025 nm/min. It has been found that surface swelling during ionizing irradiation is associated with dislocation of the microstructure or "dislocation in multilayer compounds".

7. In the BN and B_2O_3 samples, the temperature dependence of the specific heat capacity of compounds irradiated with heavy ^{132}Xe

ions with an energy of 167 MeV in the temperature range $100 \leq T \leq 300$ K at intensities 5.0×10^{12}, 5.0×10^{13}, 3.83×10^{14} ion/cm^2 was determined. After irirradiation with heavy ions, the value of the specific heat capacity increases to 0.0053 J/K×g and acquires a constant value in the temperature range from 200K to 300K. The kinetics of the change in specific heat capacity show that in the temperature range $120 \leq T \leq 300$K, B_4C increases 3.59 times when exposed to fast heavy ions, and 4.42 times for the B_6Si sample.

8. The thermodiffusion value for B_4C irradiated with fast heavy ^{132}Xe ions with an energy of 167 MeV in the temperature range of $100 \leq T \leq 300$K decreases to 0.475-0.397 cm^2/sec, respectively. The thermodiffusion value in B_6Si samples was 0.35-0.49 cm^2/sec. Heat capacity and thermodynamic functions of B_2O_3 compound in the temperature range of $100 \leq T \leq 700$K, heat capacity and thermodynamic functions of B_2O_3 compound irradiated with 162 MeV energy ^{132}Xe ions were determined, thermophysical parameters of B_4C, B_6Si, BN compounds in the temperature range of $100 \leq T \leq 1200$K. has been appointed.

9. Surface morphology study revealed that 100 nm amorphization traces and B_2O_3 surface degradation were observed on samples of boron carbide, boron silicate and boron nitride microcrystals at 194 kGy gamma absorption doses. Element mapping analysis revealed that after gamma irradiation, the atoms of the elements that make up the structure are inhomogeneously distributed and the amount of oxygen increased by 1.4% at absorption doses of 194 kGy.

10. From the main spectrophotometric spectrum of the boron carbide sample, F^+ color centers with activation energy of 1.89 eV at wavelengths of 212 nm, 300 nm, 374 nm and 434 nm, two M color centers with activation energy of 0.1 eV at 561 nm and 648 nm were found in the same absorption spectrum. As the dose of gamma irradiation increases, the absorption spectra of the F^+ color centers increase. In the absorption spectra of a boron carbide sample irradiated at an absorption dose of 48.5 kGy, new defects were detected in the absorption band at 266 nm, two new color centers, 145.5 kGy F and F^+ color centers in the wavelength range of 332-404 nm at an

absorption dose of 97 kGy. The critical oxidation temperature in B_4C and B_6Si samples irradiated with gamma quanta is 970 °C, and the percentage of oxidation in the non-isothermal region indicates the formation of a liquid B_2O_3 layer and SiO_2 on the surface of microcrystalline particles. Oxidation is 3.5% in the non-irradiated sample and 8.2% in the 194 kGy irradiated sample. The depth of oxidation at the surface is significantly dependent on the irradiation absorption dose and temperature and the formation of a layer with a maximum thickness of 60 nm.

THE MAIN RESULTS OF DISSERTATION ARE PUBLISHED IN THE FOLLOWING ARTICLES AND THESISES

1. R.Q. Qəribov, M.N. Mirzəyev, Bor karbid birləşməsinin mikrostrukturu və termik analizi, AMEA, Xəbərləri, Fizika-Texnikavə Riyaziyyat elmləri seriyası, XXXVI, №5, (2016) s.119-122.
2. M.N. Mirzəyev, R.Q. Qəribov, A.A. İbrahimov, B_6Si, B_4C və BN birləşmələrinin səth morfologiyasının tarayıcı elektron mikraskop ilə tədqiqi, Journal of Qafqaz University-Physics, №4(1), (2016) s.80-84
3. M.N. Mirzəyev, X.F. Məmmədov, R.Q.Qəribov, Q.R. Allahverdiyev, Ş.Ə. Hümbətov, Termik işlənmə sürətindən asılı olaraq B_6Si və B_4C birləşməsinin səth morfologiyası, mikrotərkibi və istilik xassələrinin tədqiqi, Bakı Universitetinin xəbərləri, №1 (2017) s.199-207.
4. M.N. Mirzayev, S.H. Jabarov, E.B. Asgerov, R.N. Mehdiyeva, T.T. Thabethe, S. Biira, N.V. Tiep, Crystal structure changes and weight kinetics of silicon-hexaboride under gamma irradiation dose, Results in Physics. 10 (2018) 541-545.
5. M.N. Mirzayev, Kh.F. Mammadov, R.G. Garibov, E.B. Askerov, Thermophysical properties of boron carbide irradiated by ionizing radiation, High Temperature 56(3) (2018) 374–377.
6. M.N. Mirzayev, R.N. Mehdiyeva, R.G. Garibov, N.A. Ismayilova, S.H. Jabarov, Influence of gamma irradiation on the surface morphology, XRD and thermophysical properties of silicide hexoboride, Modern Physics Letters B Vol. 32, №14, 1850151, 2018.
7. M.N. Mirzayev, R.N.Mehdiyeva, Kh.F.Mammadov, S.H.Jabarov, E.B.Asgerov, Calculation of the thermal parameters of boron silicide by differential sacnning calorimetry, Physics of Particles and Nuclei Letters (Physics of Solid State and Condensed Matter), 2018, Vol. 15, №. 6, pp. 673–677

8. M.N. Mirzayev, Kh.F. Mammadov, V.A. Skuratov, E. Demir, S.H. Jabarov, N.A. Ismayilova, S. Biira, B. Abdurakhimov, E. Popov, Oxidation kinetics and thermophysical properties of gamma irradiated silicon hexaboride, Journal of Alloys and Compounds, 801 (2019)151-157.
9. M.N.Mirzayev, E. Demir, K. Mammadov, R. Mehdiyeva, S. Jabarov, A.B. Tugrul, S.Biira, N. Tiep, T.Thabethe, Thermodynamics kinetics of boron carbideunder gamma irradiation dose, International Journal of Modern Physics B, Vol. 33, No. 9 (2019) 1950073.
10. M.N. Mirzayev, R.N. Mehdiyeva, S.Z. Melikova, S.H. Jabarov, T.T. Thabethe, S. Biira, M.A. Kurbanov, N.V. Tiep, Formation of Color Centers and Concentration of Defects in Boron Carbide Irradiated at Low Gamma Radiation Doses, Journal of the Korean Physical Society, Vol. 74, No. 4, 2019, pp. 363-367.
11. Matlab N. Mirzayev, Oxidation kinetics of boron carbide ceramic under high gamma irradiation dose in the high temperature, Ceramics International, 46 (3), 2816-2822, 2020.
12. Mirzayev, M.N., Demir, E., Mammadov, K.F. et al. Amorphisation of boron carbide under gamma irradiation. Pramana-Journal of Physics, 94, 110 (2020).
13. Matlab N. Mirzayev, Study thermodynamic assessment of the B-C and B-Si binary systems with swift heavy ions and high intense electron beam irradiation at the low temperature, Modern Physics Letters B, 2050395, 2020.
14. Matlab N. Mirzayev, High-flux neutron irradiation of boron trioxide analyzed with Raman and FTIR spectroscopy, International Journal of Modern Physics B, 34 (18), 2050160, 2020.
15. Matlab N. Mirzayev, E. Popov, E. Demir, B.A. Abdurakhimov, D.M. Mirzayeva, V.A. Sukratov, A.K. Mutali, V.N. Tiep, S. Biira, M.Yu. Tashmetov, K. Olejniczak, O. Kristavchuk, Thermophysical behavior of boron nitride and boron trioxide ceramics compounds with high energy electron fluence and

swift heavy ion irradiated, Journal of Alloys and Compounds, 834 (2020) 155119.
16. Matlab N. Mirzayev, Simultaneous measurements of heat flow rate and thermal properties of nano boron trioxide under neutron irradiation at the low and high temperature, Vacuum, 173, 109162, 2020.
17. M.N Mirzayev, B.A Abdurakhimov, S.H. Jabarov, M.Yu. Tashmetov, E. Demir, N.V. Tiep, N.A. Ismayilova, Y.I. Aliyev, E. Popov, D.M. Mirzayeva, S.I. Karaaslan, G.I. Georgiev, Effect of high intense electron beam irradiation on structural and Raman properties of boron carbide micro powder, International Journal of Modern Physics B, 34 (04) (2020) 2050008.
18. Matlab N. Mirzayev, Heat transfer of hexagonal boron nitride (h-BN) compound up to 1 MeV neutron energy: Kinetics of the release of wigner energy, Radiation Physics and Chemistry, 180 (2021) 109244.
19. Matlab N Mirzayev, Alexander A Donkov, Evgeni A Popov, Ertugrul Demir, Sakin H Jabarov, Levan S Chkhartishvili, Samuel A Adeojo, Aleksandr S Doroshkevich, Alexey A Sidorin, Asif G Asadov, Thabsile T Thabethe, Mayeen U Khandaker, Sultan Alamri, Hamid Osman, Alex V Trukhanov, Sergei V Trukhanov, Modeling and X-ray analysis of defect nanoclusters formation in B_4C under ion irradiation, Nanomaterials,12(15) (2022) 2644.
20. M.N. Mirzayev, Kh. Mammadov, R.N. Mehdiyeva, R.G. Garibov, BA. Skuratov, N.V. Tiep, E.B. Askerov, E. Demir, A.B. Tugrul, S.H. Jabarov, Study of atom dynamics of the (SS GRADE 321) $+B_4C+Al_2O_3$ compounds under heavy ion irradiation, Journal of Radiation Researches, 2018, No2, 5, pp.173-178
21. M.N. Mirzayev, E. Popov, E. Demir, B. Abdurakhimov, D.M. Mirzayeva, V.N. Tiep, G.I. Georgiev, A.K. Mutali, M.B. Mamatova, Thermophysical behavior of nano boron trioxide under high intense electron beam irradiation, Advanced Physical Research, 1 (2), 63-69, 2019

22. O.A. Səmədov, M.N. Mirzəyev, Sürətli ağır ion, neytron, elektron və qamma şüalanmanın təsiri nəticəsində borlu binar birləşmələrdə defekt əmələgəlmə mexanizmi və termofiziki effektlər, AJP Fizika, XXVIII, №1, (2022) s.18-30.
23. M.N. Mirzayev, Kh.F.Mammadov, R.N.Mehdiyeva, S.H.Jabarov, E.B.Asgerov, S.M. Akberova, Chances crystal structure of silicon hexaboride irradiated under gamma ray, 18th International Conference on Radiation Physics and Chemistry of Condensed Matter, EFRE-2018, September 16-22, Tomsk, Russia, 2018. P.528
24. M.N. Mirzayev, Kh.F. Mammadov, R.N. Mehdiyeva, Microstructural, macroscopic length and lattice parameters changes in gamma-irradiated boron carbide. Modern Trends in Condensed Matter Physics, MTCMP – 2018, September 24-26, Baku, Azerbaijan, 2018. P.118
25. Mirzayev M.N, Demir E, Mirzayeva D.M, Abdurakhimov B, Assessment of oxidation kinetics of boron ccarbide under gamma irradiation conditions, The Ninth International Conference "Modern Problems of Nuclear Physics and Nuclear Technologies", September 24-27, Tashkent, Uzbekistan, 2019, p. 262.
26. A. Dalcalı, I. Koçak, M.N. Mirzayev, E. Demir, V. Uglov, V. Shymanski, B. Büyük, Boron mine and assesment of Regional Development (3rd International Regional Development and The Role of Universities Symposium) November 21st-22nd, 2019/ Bandırma-Balıkesir, Turkey
27. E.P. Popov, A.N. Chernikov, A.I. Beskrovnyi, J. Waliszewski, M.N. Mirzayev, Cryostat for cooling samples in the study of low-temperature structural and magnetic phase transitions by neutron diffraction, Journal of Physics: Conference Series 1492 (1), 012054, 2020.
28. M.N. Mirzayev, Kh.F. Mammadov, D.M. Mirzayeva, V.A. Skuratov, E. Demir, E. Popov, Defects processes and formation of Wigner enthalpy in boron carbide under neutron irradiation, 7th International Conference on Energy Fluxes and Radiation

Effects, EFRE-2020, September 14-25, Tomsk, Russia, 2020. p.459.
29. E. Demir, M.N. Mirzayev, E. Popov, D.M. Mirzayeva, An experimental study on thermal properties of boron based compounds under ionization irradiation “Multidisciplinary approaches in solving modern problems of fundamental and applied sciences” 2020, Baku, Azerbaijan.
30. Kh.F. Mammadov, M.N. Mirzayev, R. Garibov, G. Allahverdiyev, Study of the processes of changing the crystal structure of boron carbide after the destruction of a nuclear reactor as a result of earthquake, Natural disasters and human life safety, 2017
31. M.N. Mirzayev, E. Popov, A.S. Doroshkevich, E. Demir, F. Mamedov, I.G. Genov, R.N. Mehdiyeva, Z.A. Sharipov, Thermic and electrical analogy of B_4C and BN under different irradiation, «РАДИАЦИОННАЯ ФИЗИКА ТВЁРДОГО ТЕЛА» Севастополь, 05-10 июля 2021 г. p.313-315.
32. S. Makatsaria, L. Chkhartishvili, M. Mirzayev, N. Barbakadze, O. Tsagareishvili, I. Jinikashvili, R. Chedia, Nanopowder h-BN:Fe(Fe_3O_4) as ^{10}B delivery agent in BNCT, ISBB2022, the 21st International Symposium on Boron, Borides and related materials related, from 5 to 9 September 2022, Paris, France.
33. N. Gogolidze, L. Chkhartishvili, M. Mirzayev, N. Barbakadze, O. Tsagareishvili, M. Buzariashvili, O. Lekasvili, R.Chedia, Preparation of sandwich-like B_4C/W neutron-shield materials, ISBB2022, the 21st International Symposium on Boron, Borides and related materials related, from 5 to 9 September 2022, Paris, France.

The defense will be held on 31 october 2022 at 14^{00} at the meeting of the Dissertation council BED 1.21 of Supreme Attestation Commission under the President of the Republic of Azerbaijan operating at the Institute of Radiation Problems of Azerbaijan National Academy of Sciences

Address: AZ1143, B.Vahabzadeh 9, Baku

Dissertation is accessible at the Institute of Radiation Problems of Azerbaijan National Academy of Sciences

Electronic versions of dissertation and its abstract are available on the official website of the Institute of Radiation Problems of Azerbaijan National Academy of Sciences

Abstract was sent to the required addresses on 28 september 2022

Signed for print: 27.09.2022
Paper format: A5
Volume: 91842 characters
Number of hard copies: 50